

2004

Numerical simulation on the fatigue life model of ball grid array solder joints

Sreevani Abbaraju
San Jose State University

Follow this and additional works at: https://scholarworks.sjsu.edu/etd_theses

Recommended Citation

Abbaraju, Sreevani, "Numerical simulation on the fatigue life model of ball grid array solder joints" (2004). *Master's Theses*. 2800.
DOI: <https://doi.org/10.31979/etd.8rc4-p6n8>
https://scholarworks.sjsu.edu/etd_theses/2800

This Thesis is brought to you for free and open access by the Master's Theses and Graduate Research at SJSU ScholarWorks. It has been accepted for inclusion in Master's Theses by an authorized administrator of SJSU ScholarWorks. For more information, please contact scholarworks@sjsu.edu.

NOTE TO USERS

This reproduction is the best copy available.

UMI[®]

NUMERICAL SIMULATION ON THE FATIGUE LIFE MODEL OF BALL GRID
ARRAY SOLDER JOINTS

A Thesis

Presented to

The Faculty of the Department of Mechanical and Aerospace Engineering

San Jose State University

In Partial Fulfillment

of the Requirements for the Degree

Master of Science

by

Sreevani Abbaraju

December 2004

UMI Number: 1431135

INFORMATION TO USERS

The quality of this reproduction is dependent upon the quality of the copy submitted. Broken or indistinct print, colored or poor quality illustrations and photographs, print bleed-through, substandard margins, and improper alignment can adversely affect reproduction.

In the unlikely event that the author did not send a complete manuscript and there are missing pages, these will be noted. Also, if unauthorized copyright material had to be removed, a note will indicate the deletion.

UMI[®]

UMI Microform 1431135

Copyright 2005 by ProQuest Information and Learning Company.

All rights reserved. This microform edition is protected against unauthorized copying under Title 17, United States Code.

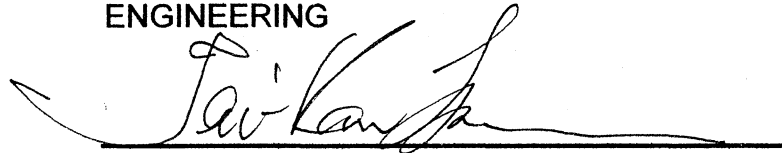
ProQuest Information and Learning Company
300 North Zeeb Road
P.O. Box 1346
Ann Arbor, MI 48106-1346

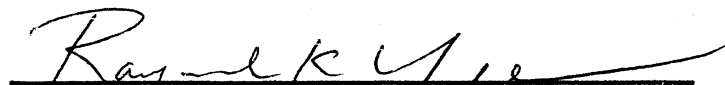
© 2004

Sreevani Abbaraju

ALL RIGHTS RESERVED

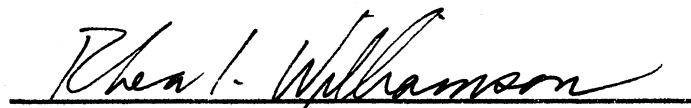
APPROVED FOR THE DEPARTMENT OF
MECHANICAL AND AEROSPACE
ENGINEERING


Dr. Tai-Ran Hsu


Dr. Raymond K. Yee


Dr. Dongji Xie, Flextronics Corporation

APPROVED FOR THE UNIVERSITY



ABSTRACT

NUMERICAL SIMULATION ON THE FATIGUE LIFE MODEL OF BALL GRID ARRAY SOLDER JOINTS

by Sreevani Abbaraju

The purpose of this thesis is to develop a model to estimate the fatigue life of Ball Grid Array (BGA) solder joints subjected to cyclic mechanical bending loads using computer simulation. It reviews the various failure modes in BGA, their causes, and regions susceptible to failure. Fundamental aspects of elastic-plastic stress analysis relevant to mechanical fatigue are reviewed for application in the model. In addition, the available fatigue models used in the reliability analysis of BGA are also studied.

Research on these aspects revealed that the strain energy density based approach is the most effective one to study the mechanical reliability of BGA. The strain energy density based approach is integrated with computer simulation and a generalized model for the estimation of fatigue life of BGA solder bumps subjected to cyclic mechanical loads has been developed.

ACKNOWLEDGEMENTS

It would have been impossible to accomplish all I did without the cooperation of my faculty, family, and friends. First and foremost I would like to thank Dr. Tai-Ran Hsu, who has been extremely supportive and ever accessible throughout the research work. I sincerely appreciate his patience in discussing even the minute and fundamental concepts involved, without which my work would never have completed. His inspiring words and valuable comments are behind the successful completion of my thesis.

I would like to extend my sincere thanks to Dr. Raymond K. Yee, who took great interest in helping me face the challenges posed by the Abaqus code during the computer simulation. I would like to specially thank him for his cooperation in accommodating my academic requests despite his tight schedule with his own students. I would also like to thank Dr. Dongji Xie who tried his best to find help in resolving the issues posed by the Abaqus code, for helping me learn to use the code, providing me the data I needed along with his valuable input from his long experience in the electronic industry.

Last but not least, I would like to acknowledge the support and understanding of my dear husband Anand, who cared for me and cooperated in all the ways he could throughout my thesis research. I would also like to thank my parents who have always been behind me with their encouraging words. Thanks to all my friends who wished me the best and inspired me to be on track.

Table of Contents

List of Figures	ix
List of Tables	xi
1 Introduction	1
1.1 Introduction to the Current Research	1
1.2 Description of the Problem	2
1.3 Introduction to Ball Grid Array Technology and its Applications in Micro Electronics	2
1.4 Applications of BGA in Micro Electronics	4
1.5 Configurations of BGA	4
1.6 Scope of the Research	5
2 Literature Survey	7
2.1 Failure Mechanisms Associated with BGA	7
2.1.1 Introduction to Failure Mechanisms in BGA	7
2.1.2 Mechanical Failure Modes and Regions Associated with BGA	8
2.1.3 Major Causes of Mechanical Failure in BGA	8
2.1.3.1 Properties of Solders	11
2.1.3.2 Failure of BGA Due to Thermal or Power Cycling	11
2.1.3.3 Failure of BGA due to Temperature Dependent Elasto-Plastic Creep	13
2.1.3.4 Failure of BGA due to Vibration	15
2.1.3.5 Failure of BGA due to PCB Bending	16
2.2 Fatigue Life Prediction Models	17
2.2.1 Coffin-Manson Equation	17

2.2.2	Continuum Damage Mechanics Method	18
2.2.3	Energy Density Based Approach	20
2.2.4	Partitioned Creep Strain Model	20
2.2.5	Matrix Creep Model	21
3	Theoretical Background	23
3.1	Fatigue of Materials	23
3.1.1	High Cycle Fatigue	24
3.1.2	Low Cycle Fatigue	25
3.2	Elastic-Plastic Stress Analysis of Solids	25
3.2.2	Basic Differences Between Elastic and Plastic Deformation of Solids	27
3.2.2	Flow Curves	27
3.2.2.1	Functional Approximation of Flow Curves	28
3.2.2.2	Functional Approximation of a Flow Curve in Multidimensional State	30
3.2.3	Yield Criteria for Multi-dimensional State	31
3.2.4	Strain Hardening	33
3.3	Elastic-Plastic Fracture Mechanics and Fatigue Fracture	35
3.3.1	Plastic Zone Corrections	35
3.3.2	Crack Opening Displacement	35
3.3.3	The J-integral	36
3.3.4	Crack Growth Resistance R-Curve	36
3.4	Finite Element Analysis	36
3.5	Application of Abaqus in Parametric Studies	37
3.5.1	Preprocessing Capabilities of Abaqus 6.4-1	37

3.5.2	Material Handling Capability in Abaqus 6.4-1	37
3.5.3	Plasticity Models in Abaqus 6.4-1	38
3.5.4	Isotropic and Kinematic Hardening in Abaqus 6.4-1	38
4	Fatigue Failure Model for BGA by Computer Simulation	40
4.1	Strain Energy Density Model	40
4.2	Methodology to Develop a Fatigue Life Model using Computer Simulation	41
4.2.1	Estimating N_0	41
4.2.2	Rate of Crack Propagation	42
4.2.3	Estimation of Critical Crack Length	42
4.2.4	Computing N_f	42
4.2.5	Developing a Generalized Model	42
4.3	Case Study	43
4.3.1	Required Information for Computer Simulation	43
4.3.2	Results of the Simulation	49
4.3.3	Developing the Model	54
5	Conclusions and Recommendation for Future Research	57
5.1	Discussion of Results	57
5.2	Advantages of the Fatigue Model Developed in the Thesis	57
5.3	Recommendation for Future Work	58
	References	59

List of Figures

Figure 1-1 Cross-sectional View of a Typical BGA Package	3
Figure 2-1 Failure Mechanisms Associated with BGA during Overstress and Wearout	8
Figure 2-2 Wire Frame Model of the Package in Thermal Cycling	11
Figure 2-3 Thermal Load Profile to which the Package is Subjected	12
Figure 2-4 Variation of Von Mises Stress with the Diagonal Distance from the Package Center	12
Figure 2-5 Critical Balls Studied as a Set of Nodes	14
Figure 2-6 Hysteresis Behavior of Solder Ball One in Thermal Creep	14
Figure 2-7 Hysteresis Behavior of Solder Ball Two in Thermal Creep	15
Figure 2-8 Stress Strain Diagrams for Cyclic Loading	19
Figure 3-1 Fatigue Crack Propagation in Polycrystalline Material Under Uniaxial Loading	24
Figure 3-2 Typical Stress-Strain Curve for a Rod under Uniaxial Tensile Test	26
Figure 3-3 Idealized Flow Curves	28
Figure 3-4 Parameters Required for Ramberg-Osgood Equation	29
Figure 3-5 Parameters for Hsu-Bertel Polynomial	30
Figure 3-6 Using Uniaxial Flow Curve for Multidimensional Analysis	30
Figure 3-7 A Two Dimensional Tresca Yield Surface	32
Figure 3-8 A Two dimensional Von Mises Yield Surface	32
Figure 3-9 Comparison of Von Mises and Tresca Criterion	33
Figure 3-10 Paths for Loading, Unloading, and Reloading for an Isotropic Hardening Solid	34

Figure 4-1 Schematic Diagram of a BGA Package	44
Figure 4-2 Schematic Representation of the Assembly	45
Figure 4-3 Quarter Model of the BGA	47
Figure 4-4 Quarter Model of Isolated Solder Balls	47
Figure 4-5 Quarter Model of the Assembly of PCB and Package	47
Figure 4-6 Step Manager in Abaqus Modeling	48
Figure 4-7 Complete Assembly with the Package at the Center of the PCB	49
Figure 4-8 Quarter Model with Associated Boundary Conditions	49
Figure 4-9 Deformed Solder Balls at 1mm Applied Displacement	50
Figure 4-10 Hysteresis Behavior of S_{cr} at 1mm Applied Displacement	51
Figure 4-11 Normal Strain vs Number of Cycles of 1mm Displacement	52
Figure 4-12 Extrapolated Curve of Normal Strain vs Number of Cycles of 1mm Displacement	52 55
Figure 4-13 Strain Energy Density per Cycle vs Number of Cycles at 1mm Applied Displacement	53 53
Figure 4-14 Fatigue Life as a Function of Strain Energy Density	55
Figure 4-15 Number of Cycles to Crack Initiation vs Strain Energy Density per Cycle	55

List of Tables

Table 1-1 Applications of Single Chip CSP	5
Table 2-1 Most Common Failure Sites in BGA	9
Table 2-2 Failure Causes, Factors, and Sites in BGA	10
Table 3-1 Differences between Elastic and Plastic Deformation	27
Table 4-1 Material Properties of Associated Materials (Flextronics Corporation)	45
Table 4-2 Fatigue Life at Various Applied Displacements	54

1 Introduction

1.1 Introduction to the Current Research

The exponential growth in microelectronics applications is stretching the capabilities of available portable electronic devices, and is urging researchers to find more reliable and durable products for consumer, medical, industrial, and military applications. The increasing use of wireless devices has further prompted the need for compact devices that are capable of performing “multiple-repeatable” tasks with high level of accuracy and reliability. The core of every wireless device is an Integrated Chip (IC) that is packaged using various techniques to perform a set of prescribed functions. Electronic Packaging is a subject open to research.

One of the most serious concerns of engineers is the fatigue failure of the solder bumps that connect the IC to the printed circuit board (PCB) in applications like wireless telephone sets. These solder balls are in the shape of spheres. They are placed in arrays and are called “Ball Grid Arrays (BGA)” in the industry. These BGA are susceptible to structural failure due to material fatigue induced by the bending of the PCB whenever the keypad is depressed and released.

The current study focuses on the mechanical bend fatigue reliability of BGA solder joints. The objective of this research is to deduce an empirical relation between the number of cycles of bending load that a BGA package can sustain before total failure.

To demonstrate an understanding of the fundamentals of electronic packaging and theories behind the failure of BGA packages, this thesis is organized into the following headings:

1. Introduction to the problem
2. Literature survey on failure mechanisms and fatigue models
3. Theoretical background on elasto-plastic stress analysis
4. Fatigue failure model to estimate the reliability of BGA
5. Conclusions and recommendations for future research

1.2 Description of the Problem

As the dimensions and weight of wireless devices decreases, packaging density increases and thickness of the PCB decreases as in plastic BGA and Chip Scale Packaging (CSP). Hence assemblies of compliant laminates are sensitive to low-frequency mechanical deflection. In a BGA package, solder balls provide both electrical and mechanical interconnection between the PCB and the IC. For example, when the keypad of a mobile phone is depressed, the corresponding PCB bends, stressing the interconnects on its tensile side. When this happens repetitively in a product's life cycle, the solder balls crack and eventually fail due to *low-frequency isothermal mechanical fatigue*. This research develops a methodology to estimate the fatigue life of solder balls subjected to cyclic isothermal mechanical bending load.

1.3 Introduction to Ball Grid Array Technology and its Applications in Micro Electronics

Leaded (legged) packages such as Dual Inline Packages (DIP), Plastic Leadless Chip Carriers (PLCC), and Quad Flat Packs (QFP) represent the bulk of all packages used today. Also known as "boundary" packages (a category that also includes leadless packages), their connections to the PCB align along the periphery of the package. They

are very popular in prototyping environments, where easy replacement of chips is desirable and in manufacturing environments that value just-in-time insertion of a chip before shipping to a customer. However, they increase system cost and impedance due to the sockets that affect their performance and signal integrity negatively.

On the other hand, Ball Grid Arrays (BGA) and Pin Grid Arrays (PGA) use surface mount technology. In this technique, as shown in Figure 1-1, silicon die is placed on a glass epoxy board, wire bonded, and hermetically sealed by means of transfer molding.

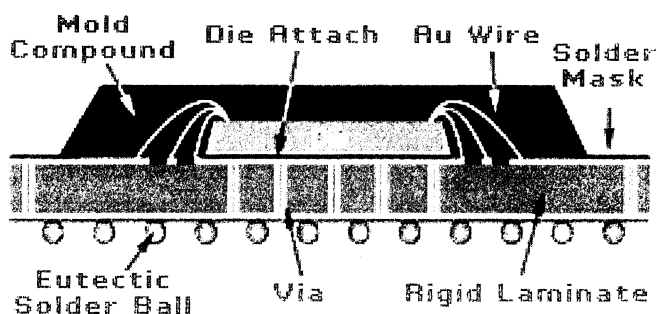


Figure 1-1 Cross-sectional View of a Typical BGA Package

Source: Reed Electronics. Retrieved February 2003, from

<http://www.reedelectronics.com/ednmag/contents/images/220402.pdf>

Contact balls or bumps are placed on the bottom of the epoxy board to form an array. These balls are usually made from alloys of tin-lead solder material. Ball or bump connections offer lower impedance than leads. As device pin count increases, an area array package offers space-efficient solutions than their boundary package counterparts. The advantages of BGA packages over other interconnections are outlined as follows:

(Intel. Retrieved September 21, 2003, from

http://developer.intel.com/design/packtech/ch_14.pdf)

1. BGA packages can be used for applications with high thermal and electrical requirements.
2. BGA solder balls fit IC into smaller footprints thereby decreasing pitch and accommodating higher density of input-output connections than the conventional QFP or PGA.
3. BGA features shorter electrical path lengths that reduce inductance.
4. Mechanical problems such as fragile leads are absent.
5. Larger spacing between solder lands provide adequate tolerances for reliable surface mounting.
6. A good part of heat dissipation can be facilitated through the substrate.
7. Small body size BGA packages come close to chip scale package size for use in limited space applications

1.4 Applications of BGA in Micro Electronics








Table 1-1 gives a brief overview of the application of Single Chip CSP (SCP) in microelectronics (Rao, 2001).

1.5 Configurations of BGA

There are different classifications of a BGA. Depending on the substrate, there are Ceramic BGA (CBGA), Plastic BGA (PBGA), Metallic BGA (MBGA), and Dimple BGA (DBGA). Based on interconnect material, there are solder balls made of 63Sn37Pb, 60Sn40Pb, 95Pb5Sn etc. The popular lead-free alloys available are 96.5Sn3.5Ag, 96.5Sn3Ag0.5Cu, 95Sn5Ag, 95Sn5Sb, 42Sn58Bi etc. Based on the technology used for

first level interconnection, there are wire bonded, tape-automated bonded, and flip-chip solder bumps.

Table 1-1 Applications of Single Chip CSP

TYPES OF CSP				
Category	Type	Example	Devices	Applications
Flex Interposer	TAB/ flip chip		Flash, SRAM, ASIC, Microcontroller, DSP	Camcorder, CellPhone, Memory Crad, Computer
	Wirebonding			
Rigid substrate	Flip Chip		Processor, Controller, DSP, SRAM, ASIC	CellPhone, Camcorder, PDA
	Wirebonding			
Lead Frame	Wirebonding		Flash, DRAM, analog IC	CellPhone, Memory Crad, Notebook
Wafer-Level Assembly	Redistribution		Memory, controllers, ASIC, sensors, op-amp, power devices	Computers, Communications
	Substrate			

Source: Figure 7.8 of Fundamentals of Microsystems Packaging by Rao R. T

1.6 Scope of the Research

This thesis will develop a methodology to estimate the fatigue life of a BGA mounted on one side of the printed circuit board subjected to cyclic mechanical bending loads. The loading is in the form of displacement in millimeters. Thermal and environmental effects are not considered. Dwell time or the load application time is not a factor because, for most BGA in portable electronic devices, the mechanical bending load will not be applied for longer periods of time. In other words, creep-induced fatigue

deformation is not considered to be serious. Failure occurs only because of the PCB bending. Also, the finite element model is developed for a single chip-on-board and not for multi-chip modules. The effects of under fill material and solder mask definition effects are neglected in the current analysis.

2 Literature Survey

The following section gives an insight into various failure mechanisms associated with a BGA package, some experimental results obtained from literature, and various fatigue life prediction models. The purpose of this section is to demonstrate the background gained during the current research.

2.1 Failure Mechanisms Associated with BGA

Failure is defined as the loss of ability of an electronic device to perform its intended function. Various statistical models like Weibull, Exponential, Gaussian, Lognormal, Binomial, and Poisson have been used with field data to predict the failure rate of electronic components. However, these models do not investigate the causes of failure and the mechanisms involved. Therefore, a physics-of-failure approach is inevitable.

2.1.1 Introduction to Failure Mechanisms in BGA

Figure 2-1 broadly classifies the various failure mechanisms in BGA depending on the stresses that cause failure during overstress and wearout mechanisms. Both overstress and wearout mechanisms can result from manufacturing, storage, and shipping conditions. The operational causes for these failures are mechanical or thermal shocks, vibrations, thermal cycles, temperature gradients, electric voltages, electromagnetic fields, humidity, dust, or chemical contamination. Referring to Figure 2-1, only mechanical failures are relevant to the context of this research. Therefore, a brief overview of the important mechanical failure modes and mechanisms is presented in the Section 2.1.2.

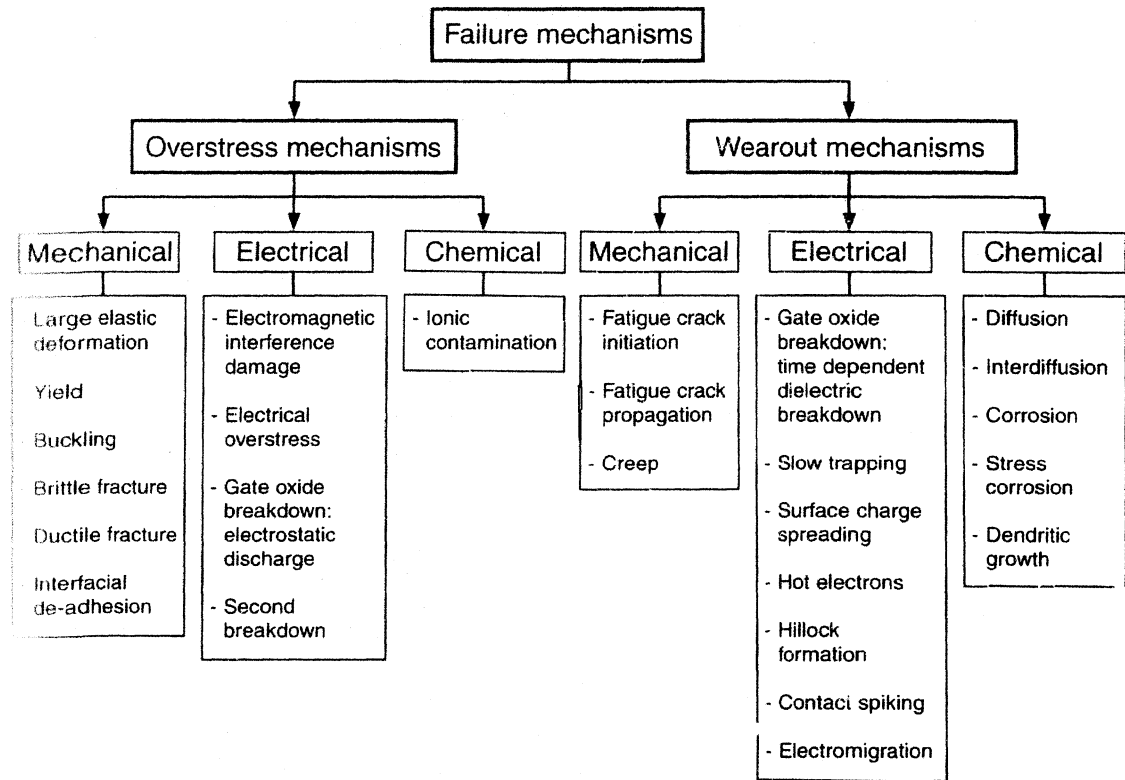


Figure 2-1 Failure Mechanisms Associated with BGA during Overstress and Wearout
 Source: Figure 3.1 of Solder Joint Reliability of BGA, CSP, Flip Chip, and Fine Pitch SMT Assemblies by Lau, J. H. and Pao, Y.

2.1.2 Mechanical Failure Modes and Regions Associated with BGA

Table 2-1 gives a list of failure sites and their locations in the package-board assembly. This list is not a comprehensive representation of all the failure regions but is helpful in providing a basic overview of the most susceptible ones.

2.1.3 Major Causes of Mechanical Failure in BGA

Table 2-2 represents the correlation between the operational causes mentioned in Section 2.1.1 and the factors that lead to ultimate failure. Although most failures begin

with a crack initiation, its subsequent propagation and ultimately failure, the parameters responsible for these stages vary by the operating condition. Before understanding the failure modes and mechanisms, it is imperative to have a basic overview of the solder material properties that make it vulnerable to failure.

Table 2-1 Most Common Failure Sites in BGA

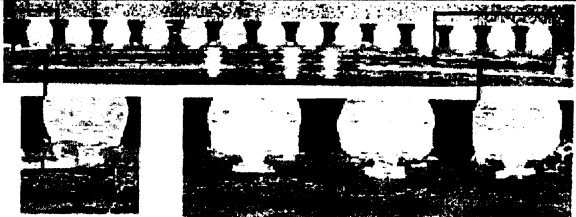
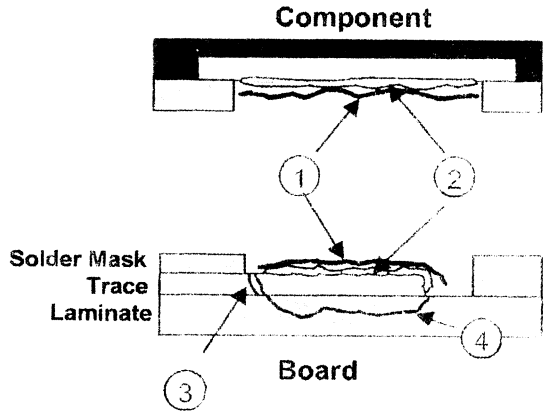
Failure site	Schematic diagram
Trace failure 2a Micro via failure 2b	 <p>2a 2b</p>
Failure in bulk solder ① Failure at the Inter metallic Layer ② Trace failures ③ PCB failures ④	 <p>Component</p> <p>Board</p> <p>Solder Mask Trace Laminate</p>

Table 2-2 Failure Causes, Factors, and Sites in BGA

Cause of failure	Factor associated	Region of failure
Thermal/Power Cycling	CTE mismatch, operating temperature range ΔT , Change in temperature with time dT/dt , duration of thermal load, stress concentration [this can be discussed as a part of CTE mismatch]	Failure in Bulk Solder and at inter-metallic
PCB bending, cyclic loading, and vibration	Plastic strain range, Accumulated stress σ , strain hardening or softening, stress concentration due to varying density, stiffness, and varying thickness within the packaged materials	Failure in Bulk Solder, Failure at inter-metallic layers, cracking of micro vias, trace and PCB failures
Shock and drop	High G's and Large displacements	Failure at inter metallic layers, trace and PCB failure, die cracking
Ball shear	Slip of crystal planes	Inter metallic or Bulk Solder

2.1.3.1 Properties of Solders

The most common solder is an alloy of tin and lead with varying compositions of each element. Eutectic solder (63Sn37Pb) has a melting point of 183°C. The melting point of the solder increases with increasing lead content. However, increasing the lead content is not a proper choice due to environmental reasons. For this reason, a two percent Silver is added to increase the strength of the alloy. Therefore, in this analysis 62Sn36Pb2Ag solder is used. The yield strength of 62Sn36Pb2Ag solder alloy is 43 MPa, Young's modulus 18 GPa, and Poisson ratio 0.4 at room temperature.

2.1.3.2 Failure of BGA Due to Thermal or Power Cycling

Thermal fatigue failure in electronic packages generally results from cracking of solder joints. For most solder alloys the operating temperatures can be as high as their melting temperature. When coupled with fatigue crack growth thermal failure becomes a dominant cause of failure in the solder joints. The following illustration (Lau and Pao, 1997) gives a qualitative approach to thermal cycling conditions of Plastic BGA.

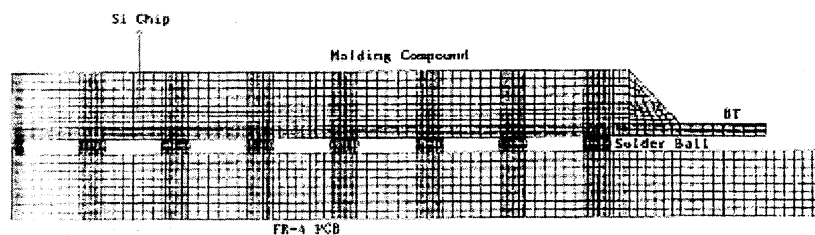


Figure 2-2 Wire Frame Model of the Package in Thermal Cycling

Source: Figure 5.20 of Solder Joint Reliability of BGA, CSP, Flip Chip, and Fine Pitch SMT Assemblies by Lau, J. H. and Pao, Y.

A 27 mm x 27 mm Plastic BGA package as in Figure 2-2 was subjected to a

thermal load profile shown in Figure 2-3. The Von Mises stress distribution in the solder balls along the diagonal direction is shown in Figure 2-4

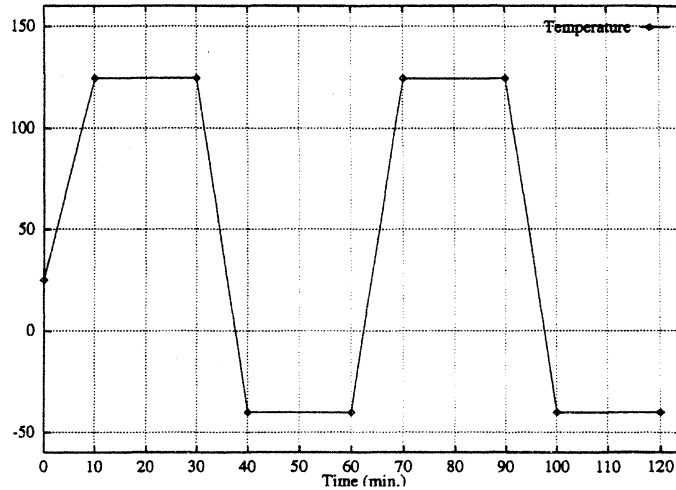


Figure 2-3 Thermal Load Profile to which the Package is Subjected

Source: Figure 5.23 of Solder Joint Reliability of BGA, CSP, Flip Chip, and Fine Pitch SMT Assemblies Lau, J. H. and Pao, Y.

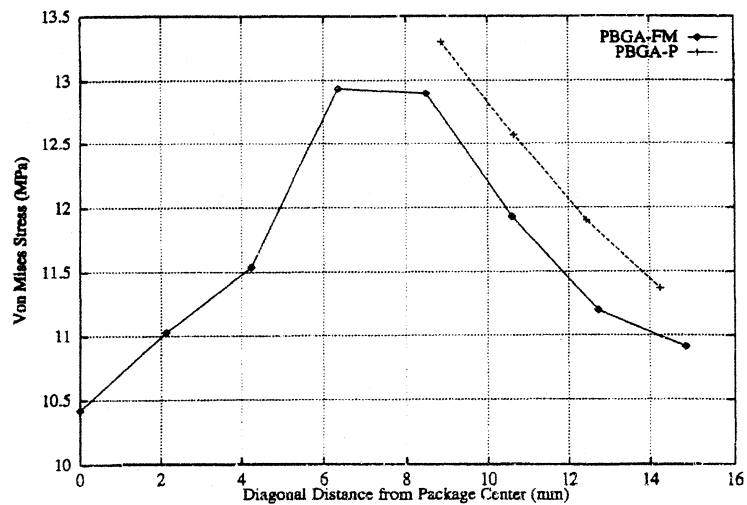


Figure 2-4 Variation of Von Mises Stress with the Diagonal Distance from the Package Center

Source: Figure 5.25 of Solder Joint Reliability of BGA, CSP, Flip Chip, and Fine Pitch

SMT Assemblies by Lau, J. H. and Pao, Y.

It is evident that the solder balls directly below the die edges have the maximum stress. This is due to the local mismatch of coefficients of thermal expansion (CTE) between the chip, epoxy molding compound, and substrate. The stresses and strains in the corner balls are very small because, the global mismatch of CTE between the substrate, molding compound, and the PCB is very small. The continuous line in Figure 2-4 represents a full-matrix BGA whereas the dotted line represents a depopulated BGA.

2.1.3.3 Failure of BGA due to Temperature Dependent Elasto-Plastic Creep

As mentioned in Section 2.1.3.2, the operating temperature of most of the BGA packages is greater than half of the solder melting temperature. When this condition exists for a long time, the package fails due to thermal creep of solder. The thermal creep behavior follows Norton's creep relation

$$(d\gamma/dt) = B \exp [\Delta H/kT] \tau^n \quad (2-1)$$

where $d\gamma/dt$ is the shear creep strain rate, n is the stress exponent which is 5.25 for eutectic solder, ΔH is the activation energy, k is the Boltzmann constant = 0.49eV for eutectic solder, B is a material constant = 0.2051/MPa-sec for eutectic solder, and T is the absolute temperature in Kelvin (Lau, 1995).

Similar to the thermal cycling results, the critical solder balls which have maximum stress and strain hysteresis responses are those right below the edges of the chip (Lau and Pao, 1997). In Figure 2-5, the chip edge is assumed to be between the two balls. Therefore, maximum stress occurs in the nodes closest to the chip edge i.e. node I at the first interface and node A at the second interface.

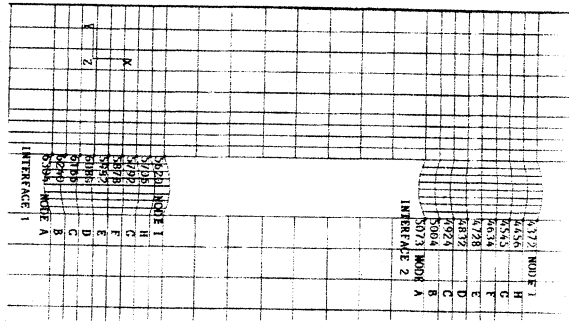


Figure 2-5 Critical Balls Studied as a Set of Nodes

Source: Figure 5.29 of Solder Joint Reliability of BGA, CSP, Flip Chip, and Fine Pitch SMT Assemblies by Lau, J. H. and Pao, Y.

When the solder balls below the chip edge are chopped into nodes for further analysis, the hysteresis behavior is as shown in Figure 2-6 and Figure 2-7.

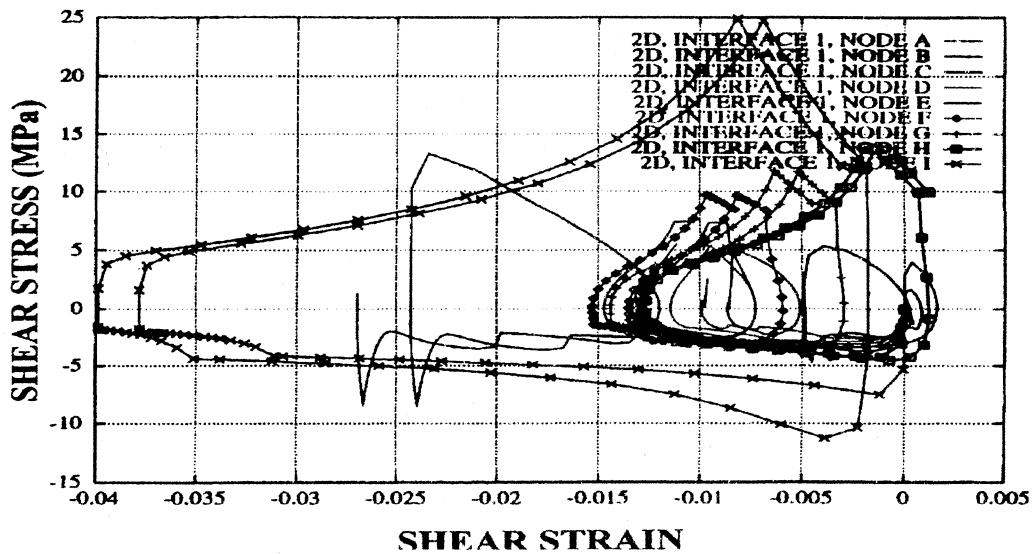


Figure 2-6 Hysteresis Behavior of Solder Ball One in Thermal Creep

Source: Figure 5.30 of Solder Joint Reliability of BGA, CSP, Flip Chip, and Fine Pitch SMT Assemblies by Lau, J. H. and Pao, Y.

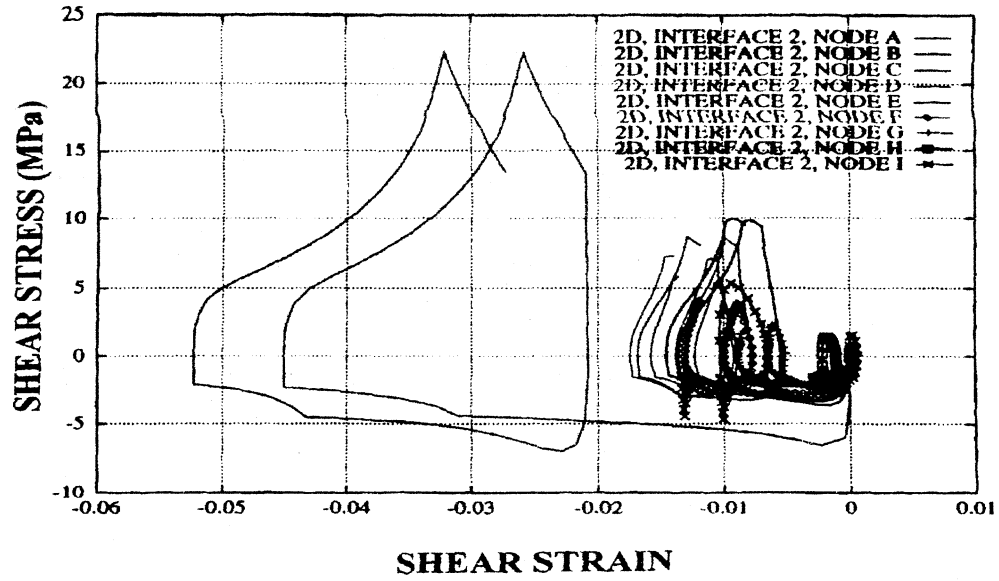


Figure 2-7 Hysteresis Behavior of Solder Ball Two in Thermal Creep

Source: Figure 5.31 of Solder Joint Reliability of BGA, CSP, Flip Chip, and Fine Pitch SMT Assemblies by Lau, J. H. and Pao, Y.

2.1.3.4 Failure of BGA due to Vibration

The US Air Force estimates that vibration and shock cause twenty-percent of total airplane electronics failure. While no generalized qualitative analysis results were available during the literature search, experimental data give an insight into the reliability of specific configurations of BGA. A series of experiments were performed by Noguchi et al. (2003) by subjecting a 62Sn36Pb2Ag to a mixed mode stress vibration with stress ratios (σ_n / τ_n) 2, 4, 5, and 6 within a frequency range of 10-25 Hz. This study indicated: the package does not have any significant amount of accumulated non-linear strain at room temperature when subjected to highcycle fatigue, the fatigue life of the package can be fitted to a line defined by

$$\tau_n = C (N_f)^{1/n} \quad (2-2)$$

where τ_n is the stress ratio, N_f is the number of cycles to failure, and C and n are material constants. The effect of frequency on highcycle fatigue life of a lead free and lead included package is insignificant in the range of 10-25 Hz, and the nominal shear stress alone is sufficient to define the fatigue life of BGA packages.

2.1.3.5 Failure of BGA due to PCB bending

Bending of PCB takes place during the operation of a keypad of a mobile phone, probe testing in the assembly line, etc. This induces both bending and shear stresses in the solder balls as well as the micro vias connecting the PCB and solder balls.

1. **Micro via failure due to PCB bending:** A Finite Element Study performed by Lim et al (2002) on a 1-2-1 built-up PCB (one micro via on one side of PCB, two conductive layers in the core of PCB, and one micro via on other surface of PCB) indicated that, the bending effects of PCB begin with the delamination of the copper traces from PCB core. Upon further loading, the copper layers stretch, yield, and eventually fracture as shown in Figure 2a of Table 2-1. This loading also causes the micro vias to lift off from the surface of the PCB and result in an electrical failure as shown in Figure 2b of Table 2-1.
2. **Solder ball failure due to PCB bending:** The low yield strength of solder material is responsible for the mechanical failure of solder balls. While no quantitative approach was available during the literature search, experiments conducted by various electronic companies have led to a common conclusion that the failure of a solder ball depends on the strain rate and hold time after package mount. Most experiments

agree with the fact that the existence of Kirkendall voids and large voids define the starting point of fracture.

3. **Solder ball failure due to mechanical impact:** Impact-induced crack is the dominant failure mode in the component drop and tumble verification tests. The solder ball that bears the impact is overstressed and the magnitude depends on the overall mechanical design and drop orientation. Unlike static or quasi-static modes, most materials under impact loading exhibit higher stiffness and material properties are strain rate dependent. Finite element simulation results discussed by Zhu (2001) suggests that during drop test, the stress induced in the solder ball farthest from the center of the component has four times the average stress during PCB bending.

2.2. Fatigue Life Prediction Models

The most commonly used models to determine the fatigue life of BGA are:

Traditional Coffin-Manson equation

Models incorporating time and temperature dependent behavior of solder joints based on one of the following mechanistic theories:

- 1) Continuum Damage Mechanics
- 2) Fracture Mechanics
- 3) Matrix Creep
- 4) Energy density based model
- 5) Partitioned creep strain based model

2.2.1 Coffin-Manson Equation

This is the simplest equation correlating plastic strain range in a load cycle to the

number of cycles the component can sustain before total failure occurs. Mathematically, the Coffin-Manson equation is

$$\Delta \varepsilon_p N^\mu = C \quad (2-3)$$

where $\Delta \varepsilon_p$ is the plastic strain range within a load cycle, μ and C are empirical constants, and N is the total number of load cycles to failure. μ corresponds to the slope of $\Delta \varepsilon - N$ curves approximately equal to two. The constant C is frequently connected with the ultimate strain ε_u in standard quasi static tension tests. The ultimate strain ε_u is connected to the relative area decrease ζ in the neck cross section, obtained from the Figure 2-8, as $\varepsilon_u = \ln(1 - \zeta)^{-1}$. Therefore the Coffin-Manson equation most often used by engineers is of the form

$$\Delta \varepsilon_p N^\mu = \ln(1 - \zeta)^{-1} \quad (2-4)$$

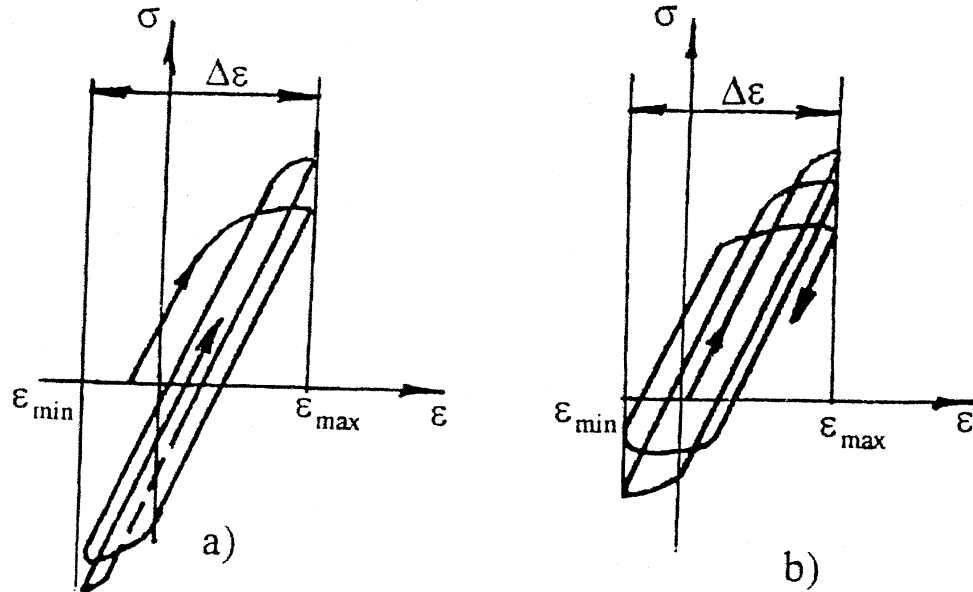
2.2.2 Continuum Damage Mechanics Method

Continuum damage mechanics is a useful tool to generalize Miner's rule by connecting the damage field/fraction to the probability of formation of even a single nucleus of the macroscopic fatigue crack in the solid domain. The approach to determine the probability of the formation of the crack is briefly discussed below. A scalar function of the local damage measure $\omega(x, N)$ is introduced, wherein x is an independent spatial variable (like a reference vector) and N is load cycle number. The limitation is that this scalar function holds a value zero for a non-damaged material and a value one for completely damaged material. Damage is said to have occurred when a first macroscopic crack is detected in the material domain. If $k(N)$ is the point-wise process of macro crack initiation in a domain say M_0 and $\mu(N)$ is its mathematical expectation i.e.,

$$\mu(N) = \mathbf{E} [k(N)] \quad (2-5)$$

Also in Equation 2-5, $\mu(N)$ is a function of the scalar function of $\omega(N)$.

$$\text{Therefore, } \mu(N) = f(\|\omega(N)\|) \quad (2-6)$$



a) Cycle Dependent Hardening Material b) Cycle Dependent Softening Material

Figure 2-8 Stress Strain Diagrams for Cyclic Loading

Source: Figure 1.8 of Mechanics of Fatigue by Bolotin, V.

The function f is differentiable with $f(0)=0$, $f(1)=1$, and $f' > 0$. Equation 2-6 corresponds to a homogenous distribution of micro damage in the domain with measure M_0 . A generalization of Equation 2-6 upon non-homogenous fields is

$$\mu(N) = \Sigma [f(\|\omega(N)\|) (dM/M_0)] \quad (2-7)$$

Poisson model also can be used to determine the probability of the formation a specific number of cracks (Bolotin, 1997).

2.2.3 Energy Density Based Approach

According to Lau (1995), the energy density based approach can be used to determine the fatigue life of BGA. Strain energy density distribution in the specimen is determined and empirically correlated to the number of cycles required to initiate primary and secondary cracks. Using Paris' law, characteristic crack growth rates for both primary and secondary cracks are obtained. Characteristic life α is computed using the equation

$$\alpha = N_{os} + \{[a - (N_{os} - N_{op}) da_p/dN] / (da_p/dN + da_s/dN)\} \quad (2-8)$$

where N_{os} and N_{op} are number of cycles to initiate primary and secondary cracks, da_p/dN and da_s/dN are crack growth rates for primary and secondary cracks respectively, and a is the critical crack length.

2.2.4 Partitioned Creep Strain Model

Although much literature was not available on this method, a summary of this technique implemented Linga Murthy et al (1997) is described below.

Large stresses result in extensive plastic deformation and large plastic strains cause an early fatigue failure in components with high compliance. The accumulated strain comprises of three parts: instantaneous elastic strain ϵ_e , time dependent creep strain ϵ_c , and time independent plastic strain ϵ_p . Mathematically,

$$\epsilon_t = \epsilon_e + \epsilon_c + \epsilon_p \quad (2-9)$$

That is,

$$\epsilon_t = \sigma/E + C1 \sigma^m + \gamma_T(1 - e^{-Bet}) + C2 \epsilon t \quad (2-10)$$

where σ is the stress, E is the temperature dependent elastic modulus, m is the reciprocal of the strain-hardening exponent, $C1$ is the reciprocal of the strength coefficient, $\dot{\epsilon}$ is the steady state creep rate, which is a function of applied stress, γ_T is the amplitude of primary creep strain, and B and $C2$ are material constants characteristic of the deformation mechanism. Each term on the right hand side of the Equation 2-10 are elastic, plastic, time dependent primary creep, and steady state creep strain components respectively.

2.2.5 Matrix Creep Model

The integrated matrix creep model uses strain range partitioning and only two creep strain components are considered. One component occurs at the grain boundaries due to sliding and the other within the solder matrix. Matrix creep component is responsible for solder fatigue and failure (Iannuzzelli and Seyyedi, 2001).

Similar to the partitioned creep strain model, the average shear strain comprises of an elastic strain, plastic strain, and a secondary creep strain component.

$$\gamma = \gamma_E + \gamma_P + \gamma_C \quad (2-11)$$

where γ is the accumulated shear strain, γ_E is the elastic strain, γ_P is the time-independent plastic strain, and γ_C is the secondary creep strain. The time-independent plastic strain is given by the following plastic flow rule:

$$\gamma_P = \left(\frac{\tau}{\tau_P(T)} \right)^2 \quad (2-12)$$

where τ_P is the temperature-dependent plasticity parameter. Finally, creep strains are obtained by integrating of the steady state creep rate equations:

$$\dot{\gamma}_C (\text{sec}^{-1}) = 8.31 \cdot \exp\left(-\frac{0.5eV}{kT}\right) \cdot \tau^2 + 1.12 \cdot \exp\left(-\frac{0.84eV}{kT}\right) \cdot \tau^{7.1} \quad (\text{with } \tau \text{ in MPa}) \quad (2-13)$$

$$\dot{\gamma}_C (\text{sec}^{-1}) = 3.952 \times 10^{-4} \cdot \exp\left(-\frac{0.5eV}{kT}\right) \cdot \tau^2 + 5.327 \times 10^{-5} \cdot \exp\left(-\frac{0.84eV}{kT}\right) \cdot \tau^{7.1} \quad (\text{with } \tau \text{ in psi}) \quad (2-14)$$

The first term on the right hand side of Equations 2-13 and 2-14 corresponds to grain boundary creep with a stress exponent $n_{GB} = 2$ and an activation energy $\Delta H_{GB} = 0.5eV$.

The second term on the right hand side corresponds to matrix creep with a stress exponent $n_{MC} = 7.1$ and an activation energy: $\Delta H_{GB} = 0.84eV$.

(National Institute of Standards and Technology. Retrieved March 29, 2004 from

http://www.metallurgy.nist.gov/solder/clech/Sn-Pb_Creep.html)

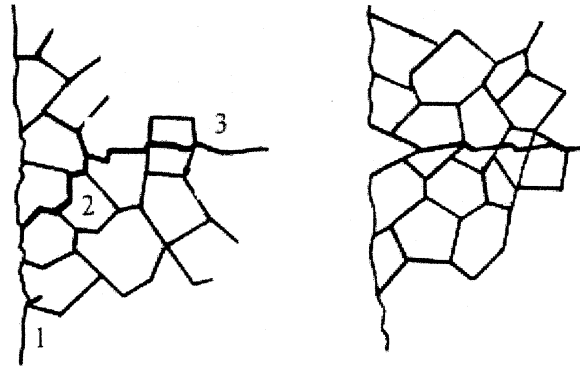
3 Theoretical Background

3.1 Fatigue of Materials

Fatigue is a gradual process of damage accumulation that proceeds on various scales beginning from the crystal lattice dislocations to the collapse of structural components. Fatigue failure proceeds in four distinct stages. In the first stage, damage accumulation is at the microstructure level along the grain boundaries and inter-granular layers. The end of this stage is distinguished by the formation of nuclei of macroscopic cracks that are formed due to the accumulation of the micro cracks that are capable of acting as stress concentrators and are susceptible to grow under similar loading. The second stage is characterized by the growth of cracks of size in the order magnitude of the grain sizes of the material. However, the depths of these cracks are small compared to the cross section of the solid specimen. These cracks, termed as “small cracks,” propagate through non-homogenous material. Most of them die away when they encounter obstacles but one or more of these cracks transform into “long cracks” that act as major stress concentrators. The final stage is the rapid propagation due to sharp stress concentration by the “long cracks” and failure of the component well below its ultimate strength.

The fatigue crack propagation is a function of the grain structure of the material under consideration. As shown in Figure 3-1 a, cracks propagate through the grains along the boundaries or in a mixed way. When the small cracks become sufficiently long, the direction of growth changes. The crack propagates into the cross section of the specimen in the opening mode. If an inherent crack exists in the form of a void or another stress

concentrator, the first two stages described in Section 3.1 do not exist. In brittle fracture mode, failure occurs suddenly without the formation of macroscopic cracks.



a) Near the Regular Surface

b) Near a Strong Stress Concentrator

Figure 3-1 Fatigue Crack Propagation in Polycrystalline Material Under Uniaxial Loading

Source: Figure 1.1 of Mechanics of Fatigue by Bolotin, V.

3.1.1 High Cycle Fatigue

High cycle fatigue is the fatigue failure under low stress levels. This type of failure occurs when the bulk stress and strain during crack propagation under cyclic loading are within the elastic range. Materials with large toughness-to-strength ratios, that display extensive plastic flow before fracture, exhibit elastic crack propagation in fatigue. In this type of failure, the first stage, the crack incubation period dominates the lifetime, while second stage may not occur until three quarters of the total life. Mathematics of fatigue growth apply only to the final quarter of the component's life. In high cycle fatigue, the crack growth rate, da/dN is proportional to the product of $\sigma^2 a$ where σ is the applied stress and a is the crack length. Stress intensity factor from linear elastic fracture mechanics

describes the resistance of the material to fracture. In high cycle fatigue there is no ductile fracture of the material and hence its mechanics can be discussed using Paris law and Griffith energy criterion for brittle fracture.

3.1.2 Low Cycle Fatigue

When crack propagation occurs within the plastic stress and strain fields caused by cyclic loading, resulting in ductile fracture, the type of failure is low cycle fatigue. The stress intensity factor K is no longer an appropriate parameter for describing the crack tip events in low cycle fatigue. Thus ΔK in Paris equation is replaced by ΔJ where ΔJ is the energy absorbed in the presence of remote plastic flow

$$da/dN = C \Delta J^m \quad (3-1)$$

where ΔJ is the work done per unit crack extension over a macroscopically small but a finite distance Δa and provides the energy available for crack extension in both elastic and elasto-plastic states. C and m are material constants. Considering the results obtained from finite element analysis in Abaqus 6.4-1 the high plastic strain values during monotonic bending of the BGA assembly implies that the type of fatigue, in this research, is low cycle fatigue.

3.2 Elastic-Plastic Stress Analysis of Solids

This discussion is relevant in this current context because of the low cycle fatigue failure under consideration, which includes cyclic elastic-plastic deformation before failure. As shown in Figure 3-2, stress-strain curve explains the behavior of the material in the elastic as well as plastic regions.

- A' = proportional limit
- A = elastic limit
- B = yield point
- m = necking point
- f = rupture point
- S_0 = yield strength of material
- S_u = ultimate tensile strength of material

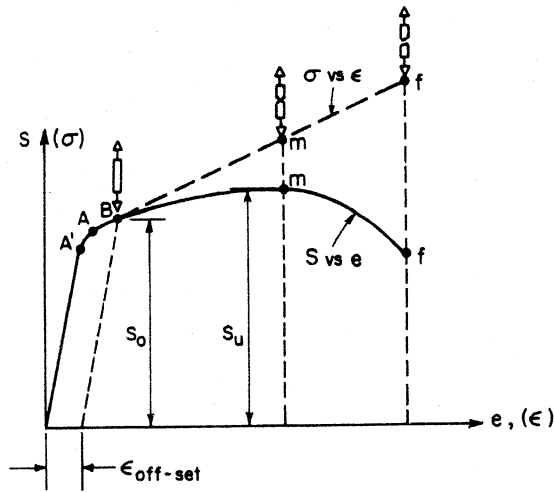


Figure 3.2 Typical stress-strain curves of a material.

Figure 3-2 Typical Stress-Strain Curve for a Rod under Uniaxial Tensile Test

Source: Modified from Figure 3.2 of The Finite Element Method in Thermomechanics by Hsu, T. R.

Elastic to plastic transition occurs at point B called the yield point. For most materials point A coincides with point B. The true stress σ and true strain ϵ curve keeps climbing until complete fracture of specimen occurs, whereas the engineering stress S Vs engineering strain e curve climbs upto the necking point and drops sharply toward the complete failure of the specimen. In almost all elastic-plastic stress analyses σ - ϵ curve is favored since the slope of the curve is positive for most engineering materials and this condition is necessary for the stability of numerical computation.

3.2.2 Basic Differences Between Elastic and Plastic Deformation of Solids

While stating a complete list of differences is impractical in this context, a few basic differences (Hsu, 1986) are listed in the Table 3-1.

Table 3-1 Differences between Elastic and Plastic Deformation

Elastic Deformation	Plastic Deformation
Small deformation with strain up to 0.1%	Large Deformation
Linear relationship between stress and strain resulting in constant stiffness of the material	Non linear relationship between stress and strain and decreasing stiffness
Completely recoverable strain after removal of applied load	Permanent deformation after the load removal
	No Volumetric change in the solid during plastic deformation with Poisson ratio at 0.5
	No dilatational change in the solid
	Total strain is a sum of elastic strain component and plastic component

3.2.2 Flow Curves

As mentioned in Section 3.2 only σ - ϵ curve is used for analysis. A flow curve represents the behavior of a material beyond the yield point.

Following curves, in Figure 3-3, are typically used in analytical solutions.

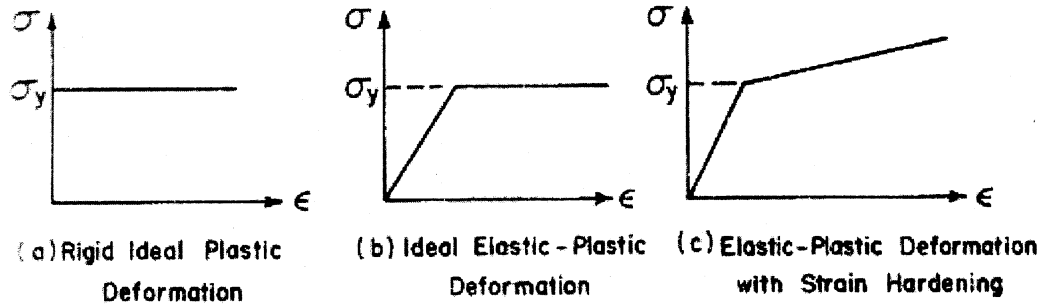


Figure 3-3 Idealized Flow Curves

Source: Figure 3.9 of The Finite Element Method in Thermomechanics by Hsu, T. R.

In most cases gradual transition from the elastic to plastic regions should be used.

3.2.2.1 Functional Approximation of Flow Curves

In elastic stress analysis stiffness of the material remains constant, whereas in plastic stress analysis a continuous variation of this property is expected as shown in Figure 3-2. A function, which can describe these curves and thus the continuous change of slopes, is called constitutive law of the material and is a necessary condition for any type of elastic-plastic stress analysis. The following two approximations provide a realistic approach to describe a gradual change from elastic to plastic region with strain or work hardening behavior.

Ramberg-Osgood equation: This equation was proposed by Ramberg and Osgood and has the form

$$(\sigma/E) + K (\sigma/E)^n \tag{3-2}$$

where n is the shape parameter $= 1 + \log\{[m_2(1-m_1)/(m_1(1-m_2))]\}/\log(\sigma_y/\sigma^1)$

and $K = \epsilon_y (E/\sigma_y)^n$ with $0 < m_1 < 1$ and $0.7 < m_2 < 1$. The case when $n \rightarrow \infty$

coincides with the flow curve representing perfect plastic materials. The major shortcomings of this approach are:

- 1) It requires the knowledge of σ_y determined at ϵ_{offset}
- 2) The curve cannot be set straight to describe approximately constant rate of work hardening exhibited by most materials beyond the initial yield point.

These shortcomings are overcome by the Hsu-Bertel's polynomial

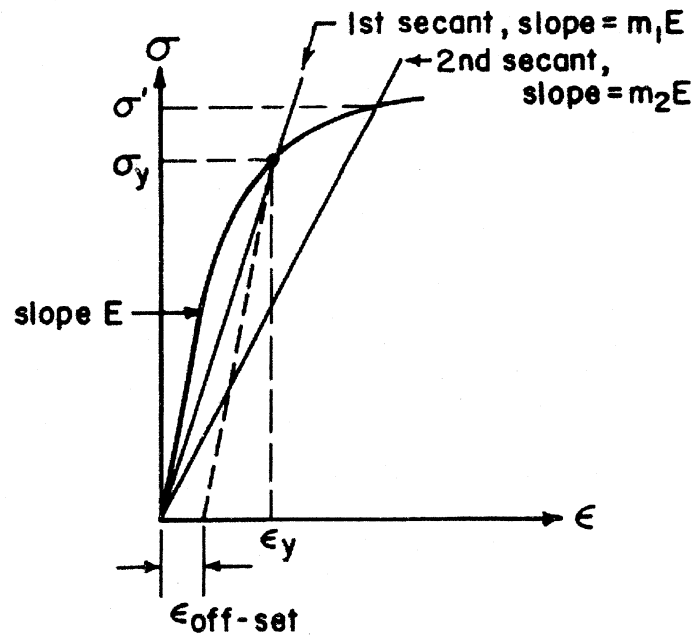


Figure 3-4 Parameters Required for Ramberg-Osgood Equation

Source: Figure 3.10 of The Finite Element Method in Thermomechanics by Hsu, T. R.

1. **Hsu-Bertel Polynomial:** This is a polynomial function, which can describe the σ - ϵ curves in a gross bilinear pattern, but with gradual elastic-plastic transition. It is mathematically expressed as

$$\sigma = E\epsilon \left\{ 1 + \left[\frac{E\epsilon}{(1 - E'/E)\sigma_k + E'\epsilon} \right]^n \right\}^{1/n}$$

where σ_k = stress level at the intersection (kink) of the elastic-plastic curve

$$n = \text{stress power or shape parameter} \\ \approx \ln 2 / \ln (\sigma_k / \sigma_0)$$

(3-3)

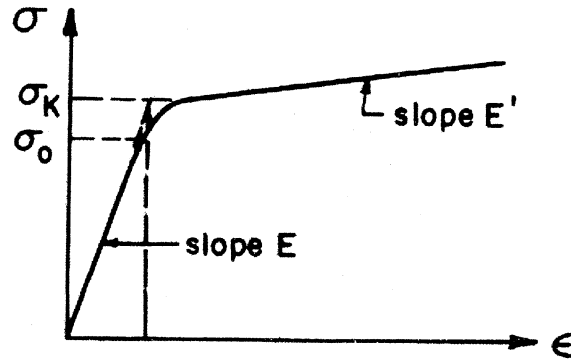


Figure 3-5 Parameters for Hsu-Bertel Polynomial

Source: Figure 3.11 of The Finite Element Method in Thermomechanics by Hsu, T. R.

3.2.2.2 Functional Approximation of a Flow Curve in Multidimensional State

To analyze a multidimensional case, uniaxial flow curve has to be modified. Figure 3-6 is the first step in this type of analysis.

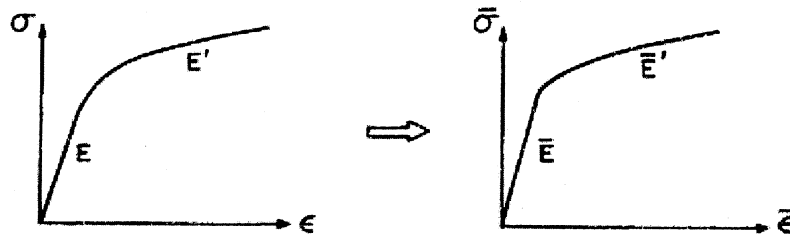


Figure 3-6 Using Uniaxial Flow Curve for Multidimensional Analysis

Source: Figure 3.12 of The Finite Element Method in Thermomechanics by Hsu, T. R.

This transformation can be achieved from the derivations given in with the following

substitutions (Cheng and Hsu, 1978)

$$\bar{E} = \frac{3E}{2(1 + \nu)} = 3G \quad (3-4)$$

$$E' = 3E' / \left[3 - \frac{(1 - 2\nu)E'}{E} \right] \quad (3-5)$$

3.2.3 Yield Criteria for Multi-dimensional State

In uniaxial tension test, yield point is defined by idealizations shown in Figure 3-2. However, for multi-dimensional cases, yield condition is defined by one of the following criteria:

1. **Tresca yield criteria:** For a solid subjected to the three principal stresses $\sigma_1, \sigma_2, \sigma_3$ the yield condition is given by

$$[(\sigma_1 - \sigma_2)^2 - \sigma_y^2][(\sigma_1 - \sigma_3)^2 - \sigma_y^2][(\sigma_2 - \sigma_3)^2 - \sigma_y^2] = 0 \quad (3-6)$$

where σ_y is the yield strength of the material from a uniaxial tension test. From Equation 3-6, we get:

$$\sigma_1 - \sigma_2 = \sigma_y \quad \text{OR} \quad \sigma_1 - \sigma_3 = \sigma_y \quad \text{OR} \quad \sigma_2 - \sigma_3 = \sigma_y$$

The Tresca yield criterion for a biaxial stress state is shown in Figure 3-7

2. **Von Mises yield criterion:** Mathematically, this criterion can be expressed as

or

$$\frac{1}{\sqrt{2}} [(\sigma_{xx} - \sigma_{yy})^2 + (\sigma_{yy} - \sigma_{zz})^2 + (\sigma_{xx} - \sigma_{zz})^2 + 6(\sigma_{xy}^2 + \sigma_{yz}^2 + \sigma_{xz}^2)]^{1/2} = \sigma_y = \sqrt{3}\sigma_s \quad (3-7)$$

$$\bar{\sigma} = \sigma_y = \sqrt{3}\sigma_s \quad (3-8)$$

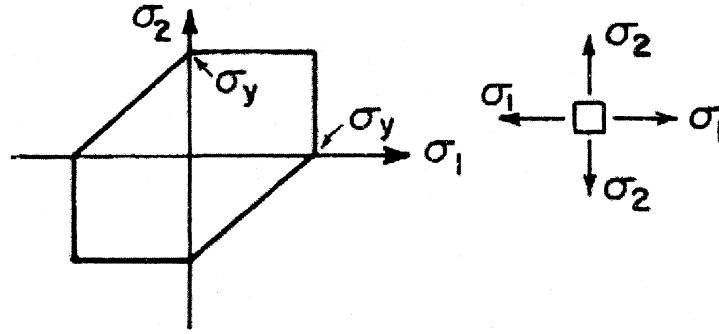


Figure 3-7 A Two Dimensional Tresca Yield Surface

Source: Figure 3.13 of The Finite Element Method in Thermomechanics by Hsu, T. R.

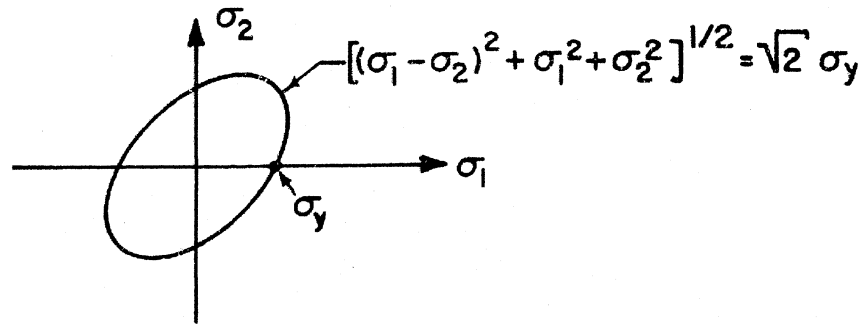


Figure 3-8 A Two dimensional Von Mises Yield Surface

Source: Figure 3.14 of The Finite Element Method in Thermomechanics by Hsu, T. R.

3. **Comparison of Tresca, Von Mises yield criteria, and experimental results:** The simplicity in mathematical expressions make Tresca criterion suitable for classical elastic-plastic problems, but the discontinuities of the function, which appear as corners in Figure 3-7, induce errors in the solution. On the contrary, the Von Mises criterion behaves as a continuous function as in Figure 3-8 while its mathematical complexity can be overcome by using finite element method. Correlation of experimental results with Von Mises yield criterion in the X1-X2 plane is shown in Figure 3-9.

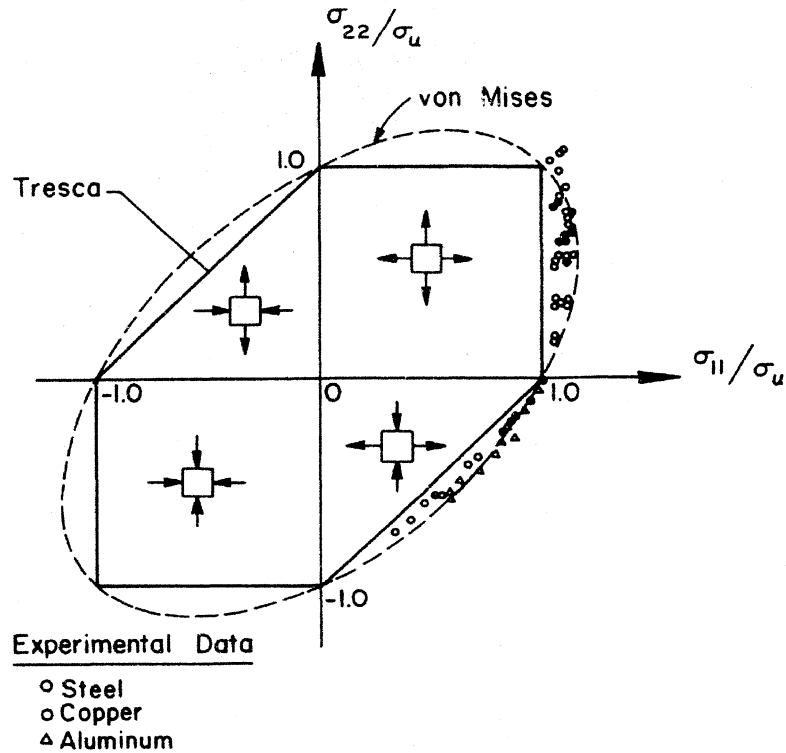


Figure 3-9 Comparison of Von Mises and Tresca Criterion

Source: Figure 3.15 of The Finite Element Method in Thermomechanics by Hsu, T. R.

3.2.4 Strain Hardening

When a material is loaded beyond its elastic limit it starts to theoretically flow without any additional load as shown in Figure 3-3b. In reality, most of the specimen retain part of its original stiffness after initial yielding. After some plastic deformation, additional load is required to produce further deformation. This phenomenon is called “work hardening” in plastic deformation. Two mathematical formulations are available for work hardening in plastic deformation. These hardening rules may produce different results in cyclic elastic-plastic loading on solids.

Isotropic hardening scheme

Referring to Figure 3-10, upon unloading from point A, which is beyond the elastic limit of the material, a permanent strain ϵ_2 is introduced in the material. During the second load cycle, the material's yield point is shifted to σ_y^1 that is greater than σ_y and coincides with the stress at the last unloading level.

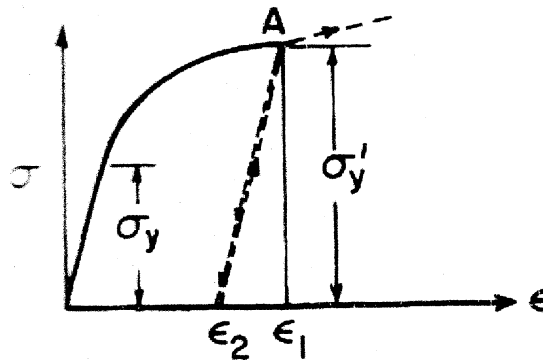


Figure 3-10 Paths for Loading, Unloading, and Reloading for an Isotropic Hardening Solid

Source: Figure 3.16 of The Finite Element Method in Thermomechanics by Hsu, T. R.

Kinematic hardening scheme:

Some materials when plastically deformed in tension, their compressive yield strength in the subsequent compression reduces by the same amount of increment in the previous tensile loading. The result is a strain hysteresis observed after a complete tension-compression load cycle. This is known as Bauschinger effect. The hardening or softening behavior is significant especially during cyclic loading as will be observed in chapter four in the case study.

3.3 Elastic-Plastic Fracture Mechanics and Fatigue Fracture

While brittle fracture usually occurs in materials with high strength to toughness ratio, ductile fracture occurs in materials like solder which is under consideration in the current research. Ductile fracture is usually associated with large plastic yield at crack tips before propagation. To solve an elastic-plastic fracture mechanics problem analytically one of the following four approaches is used

1. Plastic Zone Corrections
2. Crack Opening Displacement
3. The J-integral
4. Crack Growth Resistance R-Curve

Since the current study is not an analytical approach to fatigue fracture, the above four approaches are described briefly in the following sections.

3.3.1 Plastic Zone Corrections

This technique is an extension to linear elastic fracture mechanics except that it introduces a correction to the crack length to account for the effect of the plastic zone. The drawback of this approach is that it is applicable in problems with only low scale yielding and the limits of its applicability are uncertain.

3.3.2 Crack Opening Displacement

This technique is based on the fact that the fracture behavior in the vicinity of the crack may be characterized by the opening of the crack faces or crack opening displacement. This method can be used for cases with significant plastic flow around the

crack tip. However, under plane stress conditions the initial and maximum opening displacement are geometry dependent.

3.3.3 The J-integral

The J integral is defined as the strain energy release rate per unit crack extension to the crack tip and is expressed as a path independent contour integral. Because of this the contour required to obtain such release rate may be chosen anyway from the crack tip in order to avoid the complex deformations that normally exist in that zone. While it is applicable to a wide variety of problems involving elastic-plastic fracture, its application in cyclic loading conditions has not been clearly established.

3.3.4 Crack Growth Resistance R-Curve

The concept of crack growth resistance curve is based on the observation that during fracture of most of the sheet metals, unstable fracture is always preceded by a certain amount of stable crack growth under a monotonically rising load. This approach can be used when experimental data is available concerning crack growth and stress intensity factors.

3.4 Finite Element Analysis

All the above approaches to elastic-plastic fracture mechanics involve complex mathematics with nonlinear boundary conditions, material properties, and complicated geometry. Numerical simulation using finite element analysis is a viable approach in such a situation. Abaqus 6.4-1 is used to demonstrate the applicability of the model developed in this research with the help of a case study.

3.5 Application of Abaqus in Parametric Studies

Sections 3.5.1 through 3.5.3 present a few of the capabilities of Abaqus code in handling elastic-plastic analysis that is relevant to the current study. While Abaqus can handle a wide variety of problems it is impractical to describe them here.

3.5.1 Preprocessing Capabilities of Abaqus 6.4-1

The code has the ability to model complex geometry through its Graphical User Interface (GUI) or by importing parts and assemblies from other CAD programs like Pro-Engineer.

3.5.2 Material Handling Capability in Abaqus 6.4-1

The code can accommodate the non-linearity in material properties through its GUI or keywords dialog. The materials that can be used in Abaqus' analyses are those:

1. That exhibit pure elastic response, possibly with some energy dissipation during rapid loading by viscoelastic response. For example, elastomers like rubber or solid propellant.
2. That yield and exhibit considerable ductility beyond yield point. For example, mild steel and commonly used metals, ice at low strain rates, and clay
3. That flow by rearrangement of particles that interact generally through some dominant frictional mechanism. For example, sand.
4. That are brittle. For example, rocks, concrete, ceramics, etc.

The constitutive library provided in Abaqus contains a range of linear and nonlinear material models for all of the above categories of materials. Abaqus/Standard also

contains a user subroutine called UMAT that allows the user to input the custom material properties.

3.5.3 Plasticity Models in Abaqus 6.4-1

Abaqus uses incremental plasticity theory. Plasticity models can be implemented as strain rate-independent models or as strain rate-dependent models. A rate-independent model is one in which the constitutive response does not depend on the rate of deformation. For instance, the response of many metals at low temperatures relative to their melting temperature and at low strain rates is effectively rate-independent. In a rate-dependent model, the response does depend on the rate at which the material is strained. Examples of such models are the metal "creep" model and the rate-dependent plasticity model that is used to describe the behavior of metals at high strain rates. Because these models have similar forms, their numerical treatment is based on the same technique.

3.5.4 Isotropic and Kinematic Hardening in Abaqus 6.4-1

Isotropic hardening means that the yield function is written as:
 $f(\sigma) = \sigma^0(\epsilon^{pl}, \theta)$, where σ^0 is the equivalent (uniaxial) stress, ϵ^{pl} is the equivalent plastic strain, and θ is the temperature. Isotropic hardening is generally considered to be a suitable model for problems in which the plastic straining goes well beyond the incipient yield state where the Bauschinger effect is not noticeable. Therefore, this hardening theory is used for such applications as dynamic problems involving finite strains, manufacturing processes involving large plastic strain, and problems where plastic strain does not reverse direction. Some cases, such as low-cycle fatigue situations, involve relatively low amplitude strain cycling. In these cases it becomes important to model the

Bauschinger effect. Kinematic hardening is the simplest theory that does this. Abaqus offers a linear kinematic and a nonlinear isotropic/kinematic hardening model for such cases. [Abaqus online documentation]

4 Fatigue Failure Model for BGA by Computer Simulation

4.1 Strain Energy Density Model

The problem under consideration is the determination of fatigue life of BGA solder bumps subjected to cyclic mechanical bending loads. Most of the available fatigue models used for evaluating BGA failure were studied during the literature survey and are briefly described in Section 2.2. Strain energy density model, as described in Section 2.2.3, is the most viable model for the determination of fatigue life of BGA solder bumps.

The energy-based model predicts characteristic life in terms of the number of cycles to crack initiation, rate of crack growth, and critical crack length. The number of cycles to crack initiation is a function of strain energy density per cycle with a general form,

$$N_0 = \Delta W^\alpha \quad (4-a)$$

where N_0 is the number of cycles to initiation, ΔW is the strain energy density per cycle, and α is a constant that has to be determined from a series of experiments. Rate of crack propagation is also a function of strain energy density with a general form,

$$(da/dN) = \beta \Delta W \quad (4-b)$$

where “ da/dN ” is the change in crack length per cycle, ΔW is the strain energy density per cycle of load, and β is a constant to be determined from a series of experiments. The values of N_0 and da/dN along with critical crack length (a_{cr}) define the characteristic life

N_f as

$$N_f = N_0 + \{a_{cr} - [N_0 * (da/dN)]\} / (da/dN) \quad (4-c)$$

From Equations 4-a, 4-b, and 4-c it is evident that, to develop a fatigue life model of an element, it is imperative to conduct a series of experiments to estimate the values of the constants α and β . Also, large amount of data has to be generated from experiments and physical testing using special equipment and set up. This is time-consuming and expensive. Alternatively, a strain energy density based fatigue life model using computer simulation is developed in this thesis research.

The advantage of using computer simulation in the model is that the required data can be generated without destructive testing of the samples in less time and low cost.

4.2 Methodology to Develop a Fatigue Life Model using Computer Simulation

An overview of the methodology developed is described below followed by a case study. An assembly of PCB and BGA is modeled using a finite element code capable of performing nonlinear elastic-plastic stress analysis. Cyclic loading in the form of displacement is applied along the centerline of the PCB, simulating the three-point bending test setup. Kinematic hardening rule, discussed in Section 3.2.4, is used to describe the behavior of the solder material in cyclic loading. Parameters like yield stress, stiffness, and Poisson ratio are supplied from the stress-strain curve of the solder material.

4.2.1 Estimating N_0

The failure data for solder material is available in the form of plastic strain accumulated at ductile fracture. Therefore, accumulated plastic strain at the end of each cycle is recorded from the computer simulation. It is observed that the variation in plastic strain is fairly linear. Therefore, extrapolation of this curve is a reasonable approach to

determine the number of cycles to reach the rupture strain (available from the stress-strain curve of a material). This extrapolation leads to the estimation of an important parameter namely, “Number of cycles to crack initiation” N_0 of Equation 4-a.

4.2.2 Rate of Crack Propagation

The rate of crack propagation da/dN as a function of strain energy density can be derived in a similar manner by performing a fracture mechanics study using a finite element code on the same assembly. The strain energy density ΔW required to propagate a crack for every cycle is recorded and this data is plotted with ΔW on x-axis and da/dN on y-axis. A curve fitted to these data points gives the rate of crack propagation as a function of strain energy density as in Equation 4-b.

4.2.3 Estimation of Critical Crack Length

To determine the critical crack length, it is assumed that two cracks initiate at either ends of a solder ball near the intermetallic region (at the copper interface) at the rupture strain value. Delamination occurs when these cracks propagate towards the center of the ball and traverse a distance equal to the radius of the solder ball. Therefore, it is assumed that critical crack length is equal to the radius of the solder ball.

4.2.4 Computing N_f

Once N_0 , da/dN , and a_{cr} are computed, these values can be substituted into Equation 4-c and the characteristic life is estimated.

4.2.5 Developing a Generalized Model

The procedure described in Sections 4.2.1 through 4.2.4 is repeated for different values of strain energy density. The data points plotted with ΔW on x-axis and fatigue

life N_f , estimated using Equation 4-c, on the y-axis gives the fatigue life model for the specific assembly of the PCB and BGA under consideration without performing the physical experiments.

This method is subtly understood with the following case study considering 62Sn36Pb2Ag in Section 4.3.

4.3 Case Study

The purpose of this case study is to demonstrate the application of the model developed in Section 4.2.5. The following case study is performed on an assembly with a specific geometric configuration, material, loading, and boundary conditions.

The steps involved in estimating the fatigue life of the assembly are:

1. Modeling the assembly using the preprocessing capabilities of Abaqus 6. 4-1
2. Generating the results comparable to the failure data which is in terms of accumulated normal strain over a number of load cycles
3. Integrating these results to the model described in Section 4.2.5

4.3.1 Required Information for Computer Simulation

- Geometry:

A BGA package as shown in Figure 4-1 is soldered to a printed circuit board (PCB) 90mm long, 74mm wide, and 1mm thick. The PCB is simply supported along its short edges. Ten cycles of displacement of magnitude 1, 2, 3, and 5mm are applied on the same assembly. Due to symmetry in loading and geometry, only one quarter of the complete assembly is used in finite element modeling.

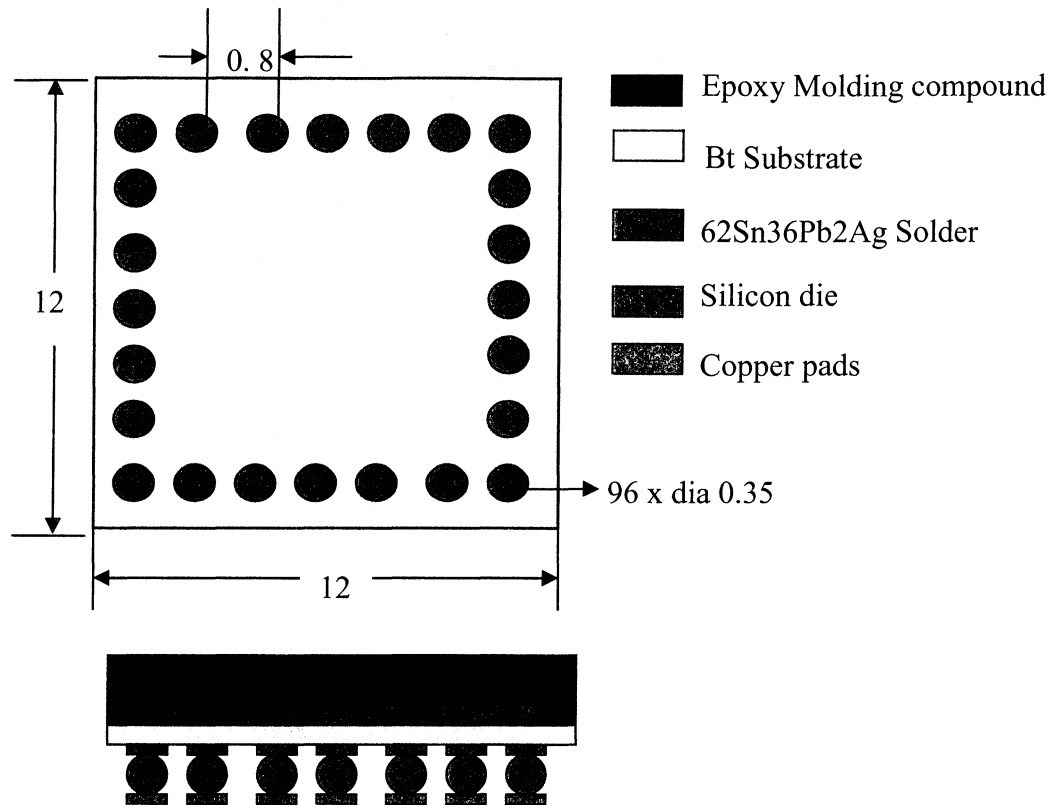


Figure 4-1 Schematic Diagram of a BGA Package

The PCB is deflected along the line passing through the center of the long edge while the short edges are simply supported as in Figure 4-2.

- Material properties:

The materials used in this study are 62Sn36Pb2Ag for the solder, FR-4 for the the PCB, Epoxy Molding compound (EMC) for the attached integrated circuits (IC), Silicon for the IC die, Copper for the solder pads, and Bt for the substrate.

The material property data obtained from multiple sources is given in Table 4-1 and the subsequent paragraph. All materials except solder are treated as elastic materials only. Therefore, any subsequent plastic deformation is in the solder only.

Table 4-1 Material Properties of Associated Materials (Flextronics Corporation)

Material	Young's Modulus(Mpa)	Poisson Ratio
Molding Compound	8960	0.3
FR-4	19499	0.4
Silicon	31000	0.4
Copper	128780	0.3
Bt substrate	20000	0.3

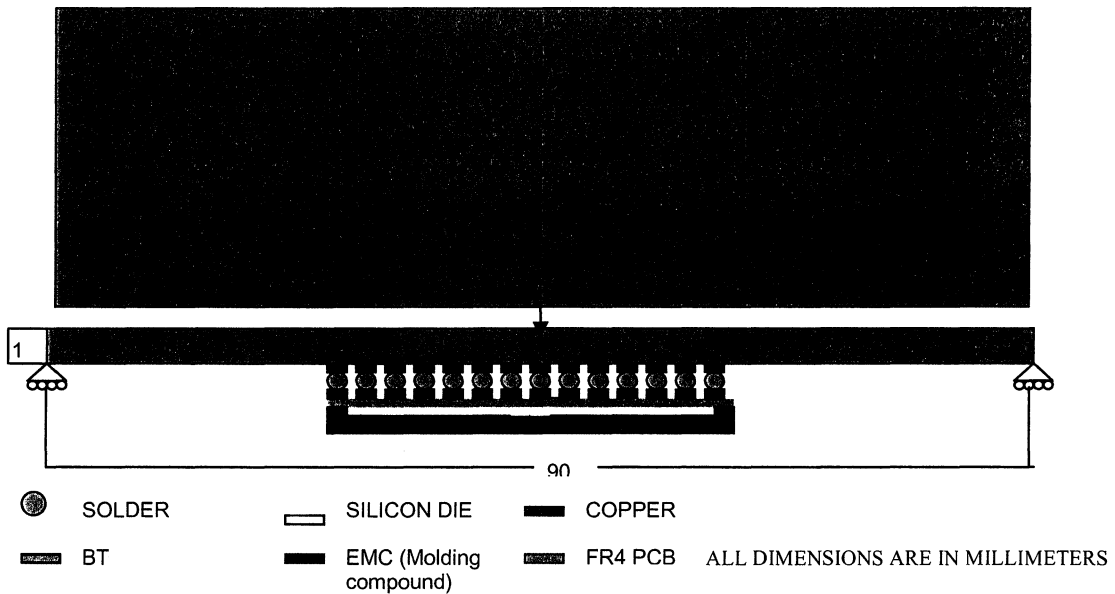


Figure 4-2 Schematic Representation of the Assembly

62Sn36Pb2Ag solder material properties

(National Institute of Standards and Technology. Retrieved March 29, 2004 from

<http://www.boulder.nist.gov/div853/lead%20free/Part1.html#%201.1>)

Young's modulus: 18000 MPa

Poisson Ratio: 0.25

Yield Strength: 43.3 MPa

Hardening exponent: 0.011

Strain at ductile fracture: 0.31

Rate at which hardening drops: 1 (Assumed value)

- **Parts and Assembly:**

The package and PCB are modeled as individual parts and the package is assembled at the center of the PCB. Figure 4-3 shows the quarter model of the BGA package used in Abaqus 6.4-1 and Figure 4-4 shows the solder balls isolated from the rest of the package.

- **Loading Steps:**

Each loading or unloading instance is modeled as a "time-invariant analysis step" starting from state 0 to 1 and the magnitude of the increment is determined by Abaqus solver. The final state of the model at the end of one load step is considered as the initial state of the model in a subsequent unload step. Each load-unload sequence is a load cycle. Ten such cycles were applied to the assembly in the current simulation. The Figure 4-6 shows the step manager in the simulation.

- **Load and Boundary Conditions:**

Due to symmetry in geometry and loading only a quarter model is considered. Therefore two boundary conditions along the faces of symmetry constrain

translation along and rotation about the axis normal to symmetric plane. Since Abaqus provides only point or edge loads and does not have a provision to apply

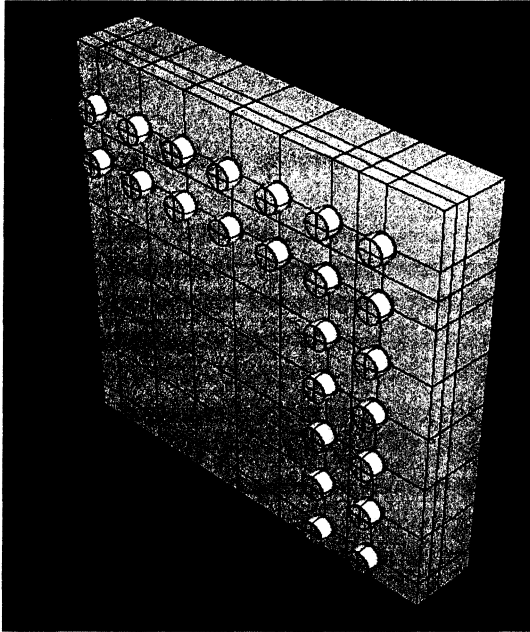


Figure 4-3 Quarter Model of the BGA

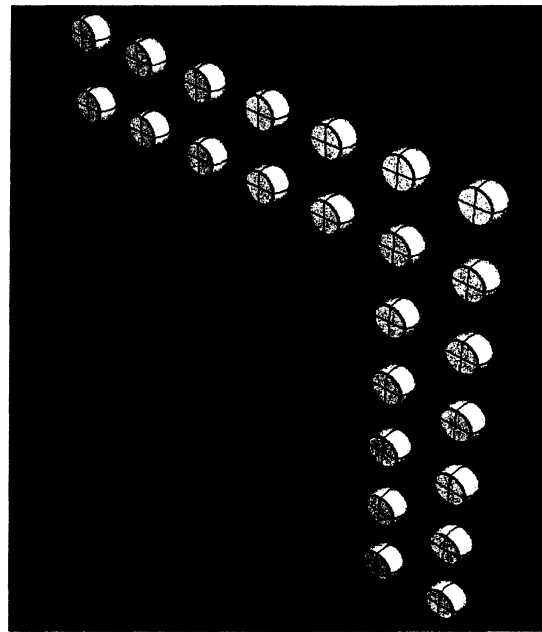


Figure 4-4 Quarter Model of Isolated Solder Balls



Figure 4-5 Quarter Model of the Assembly of PCB and Package

a displacement load, this condition is simulated by applying a boundary condition of displacement each 1mm, 2mm, 3mm, and 5mm along the centerline parallel to the width of the PCB. Figure 4-7 shows the complete model of the assembly with the package in

the center and a deflection d applied along the centerline parallel to width. The quarter model under consideration is bounded within the yellow dashed lines and is represented individually in Figure 4-8. When a quarter model is considered, the boundary conditions are as shown in Figure 4-8.

Name	Procedure	Nlgeom	Time
Initial	(Initial)	N/A	N/A
load1	Static, General	ON	1
unload1	Static, General	ON	1
load2	Static, General	ON	1
unload2	Static, General	ON	1
load3	Static, General	ON	1
unload3	Static, General	ON	1
load4	Static, General	ON	1
unload4	Static, General	ON	1
load5	Static, General	ON	1
unload5	Static, General	ON	1
load6	Static, General	ON	1
unload6	Static, General	ON	1
load7	Static, General	ON	1
unload7	Static, General	ON	1
load8	Static, General	ON	1
unload8	Static, General	ON	1
load9	Static, General	ON	1
unload9	Static, General	ON	1
load10	Static, General	ON	1

Figure 4-6 Step Manager in Abaqus Modeling

- Mesh and Element type:

The type of element used is hexahedral and is automatically generated by Abaqus

6.4-1.

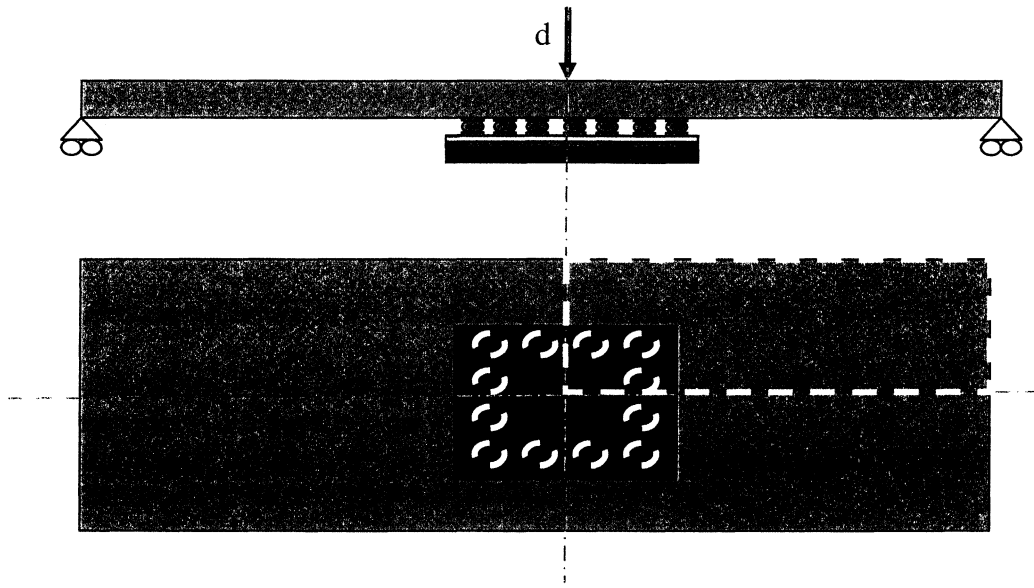


Figure 4-7 Complete Assembly with the Package at the Center of the PCB

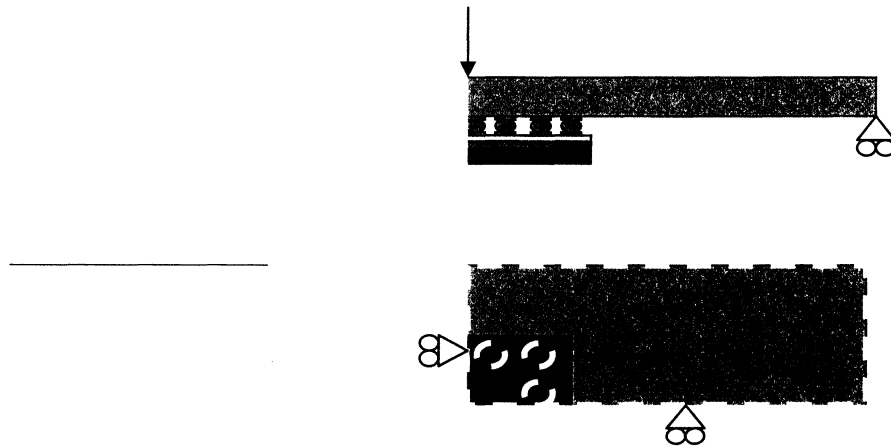


Figure 4-8 Quarter Model with Associated Boundary Conditions

4.3.2 Results of the Simulation

The data in Section 4.3.1 is given as input to Abaqus code and ten cycles of load was applied (simulated) to the assembly. A fundamental observation from the results of the simulation was that the element most susceptible to failure is the same irrespective of

the magnitude of the applied load. This element happens to be the one that is farthest from the neutral point. In Figure 4-9, the critical ball is labeled as S_{cr} .

Estimating N_0

When ten cycles of 1mm displacement are applied at the center of the package, the deformed shape of the solder balls is as shown in Figure 4-9.

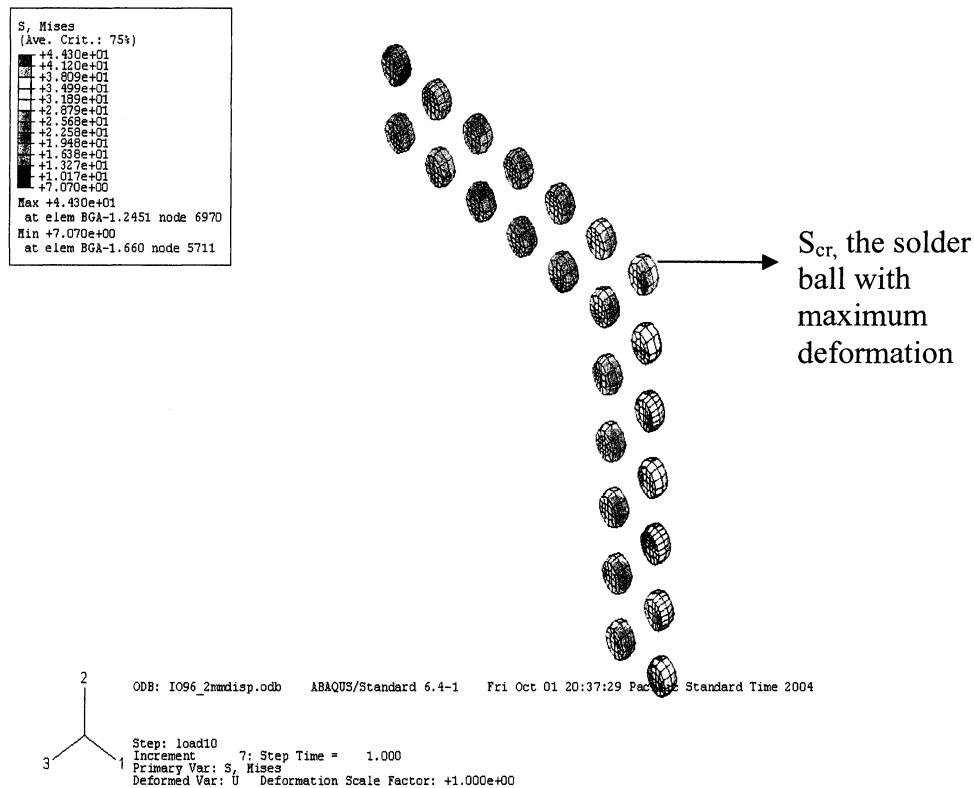


Figure 4-9 Deformed Solder Balls at 1mm Applied Displacement

The hysteresis behavior of S_{cr} is plotted in Figure 4-10. The plot of accumulated normal strain for the first ten cycles is shown in Figure 4-11. Figure 4-11 also shows that the variation in accumulated normal strain at the end of each cycle follows a fairly linear pattern beyond the fourth cycle. Thus linear extrapolation of this curve is a reasonable

approach to estimate the number of cycles to reach the rupture strain of 0.31 following the procedure described in Section 4.2.1.

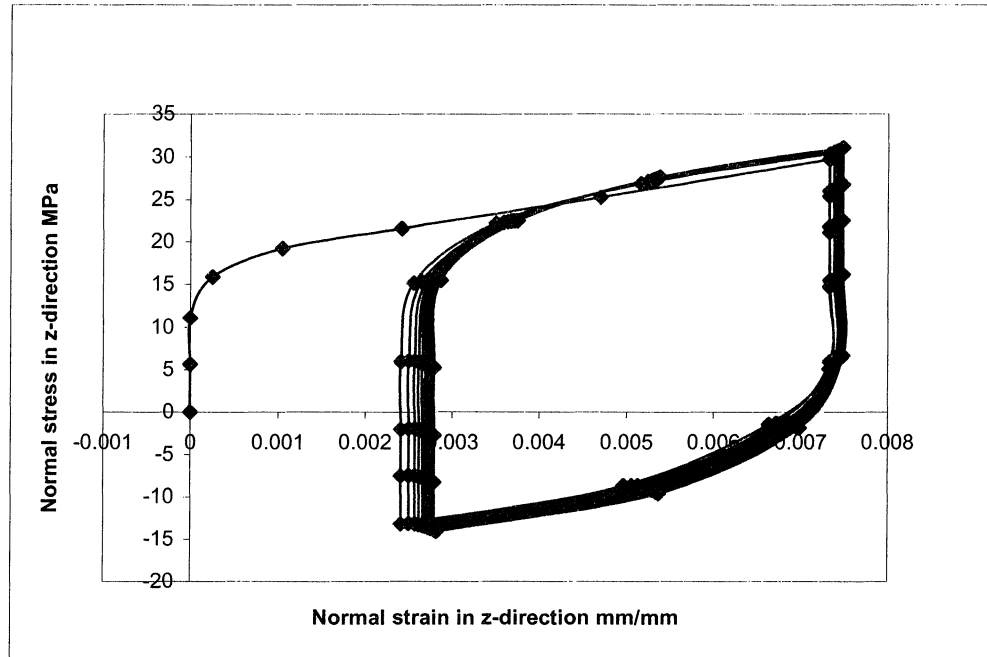


Figure 4-10 Hysteresis Behavior of S_{cr} at 1mm Applied Displacement

From Figure 4-12, it is clear that the accumulated strain reaches the value at rupture after approximately 7800 cycles. Therefore, number of cycles to crack initiation N_0 in this case is 7800 cycles.

Computing da/dN

Conservatively, it is assumed that two cracks originate at the ends of the solder ball near the intermetallic region of copper and solder. The rate of propagation of the hence formed cracks is given in equation 4-1 (Lau, 1997):

$$da/dN = 4.96 \text{ E-}8 \Delta W^{1.13} \quad (4-1)$$

where da/dN is the change in crack length per cycle and ΔW is the strain energy density

per cycle in psi. When the applied displacement is 1mm, strain energy density per cycle ΔW stabilizes at approximately 0.018 MPa or 2.6 psi from Figure 4-13.

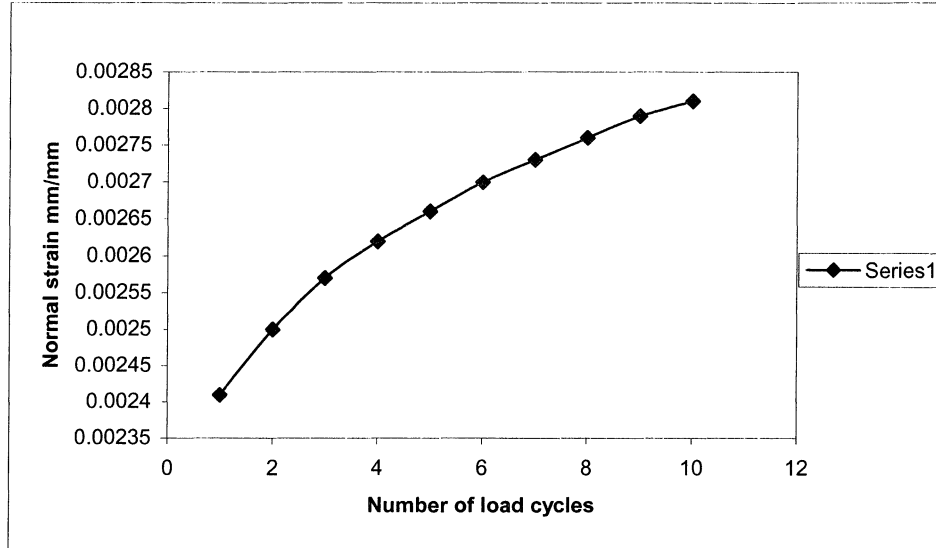


Figure 4-11 Normal Strain vs Number of Cycles of 1mm Displacement

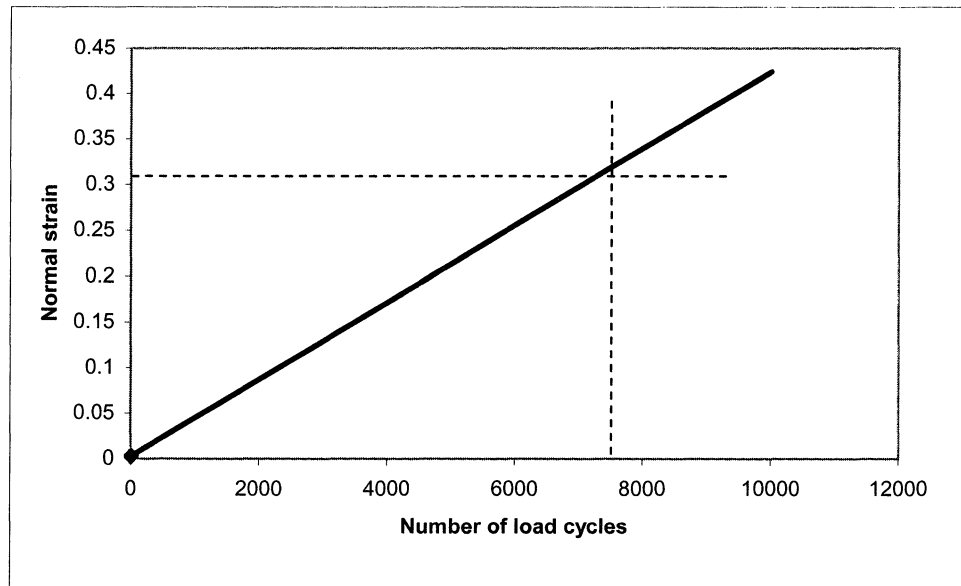


Figure 4-12 Extrapolated Curve of Normal Strain vs Number of Cycles of 1mm Displacement

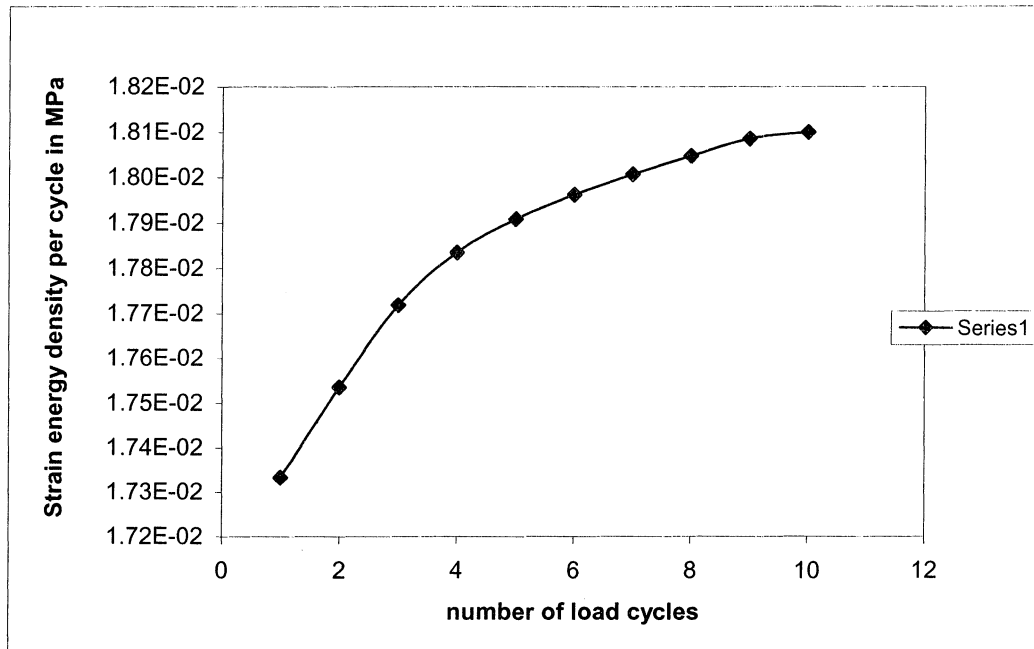


Figure 4-13 Strain Energy Density per Cycle vs Number of Cycles at 1mm Applied Displacement

When this value of ΔW is substituted in Equation 4-1, the rate of crack propagation da/dN is computed to be $14.66E-8$ inch/cycle.

4. 3. 2. 3 Computing critical crack length

To estimate “ a_{cr} ”, it is assumed that the solder ball fails completely when each crack beginning from either end of the solder ball reaches the center. Therefore, a_{cr} is same as the radius of the solder, which is 0.175 mm or 0.0069 inch.

4. 3. 2. 4 Estimating N_f

The equation to determine the characteristic life of the solder ball is given in Equation 4-2 (Lau, 1997)

$$N_f = N_o + \{[a_{cr} - N_o * da/dN] / (da/dN)\} \quad (4-2)$$

where N_o is the number of cycles to initiate a crack, da/dN is the crack growth rate in

inch/cycle, and “ a_{cr} ” is the critical crack length.

Substituting $N_0 = 7800$, $da/dN = 14.66E-8$ inch per cycle, and $a_{cr} = 0.0069$ inch in Equation 4-2, characteristic life or fatigue life N_f when a displacement of 1mm is applied to the assembly is estimated to be 47066 cycles approximately.

4.3.3 Developing the Model

By changing the applied displacement to 2mm, 3mm, and 5mm, the magnitude of strain energy density can be varied. The steps mentioned in Section 4.3.2 are repeated and, the magnitude of strain energy density and fatigue life are computed as mentioned in Table 4-2. The data from Table 4-2 is plotted to determine a relation between strain energy density and fatigue life as in Figure 4-14. Figure 4-15 relates the number of cycles to crack initiation to the strain energy density per cycle in psi.

Table 4-2 Fatigue Life at Various Applied Displacements

Applied displacement (mm)	Strain energy density in psi	Number of cycles for crack initiation	Fatigue life in cycles
1	2.6	7800	47066
2	8.34	850	12639
3	28.98	280	3093
5	101.5	45	750

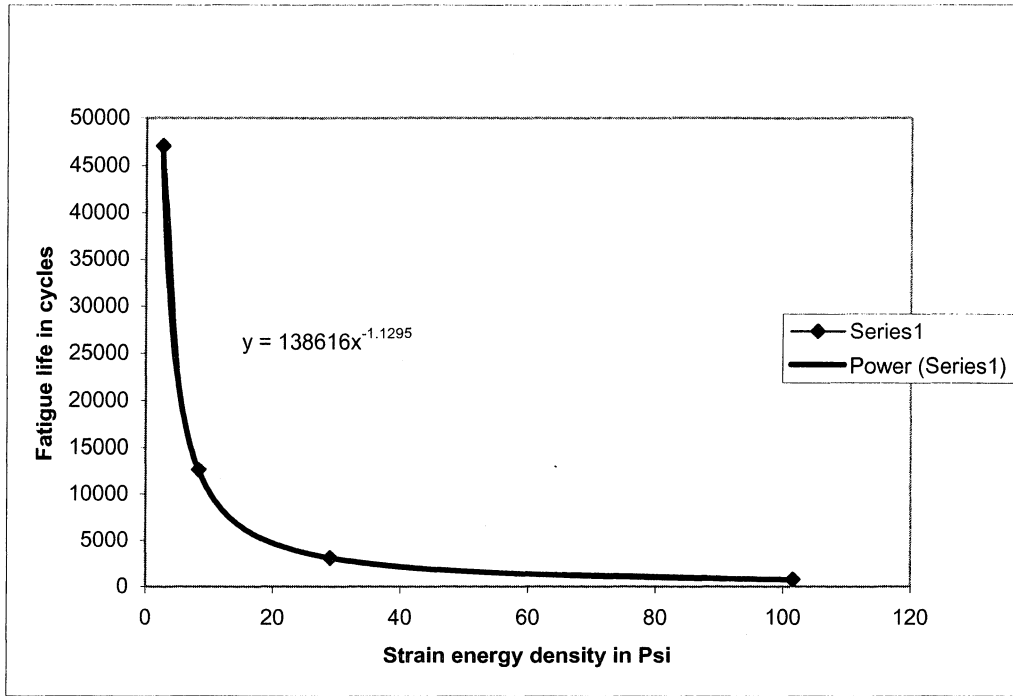


Figure 4-14 Fatigue Life as a Function of Strain Energy Density

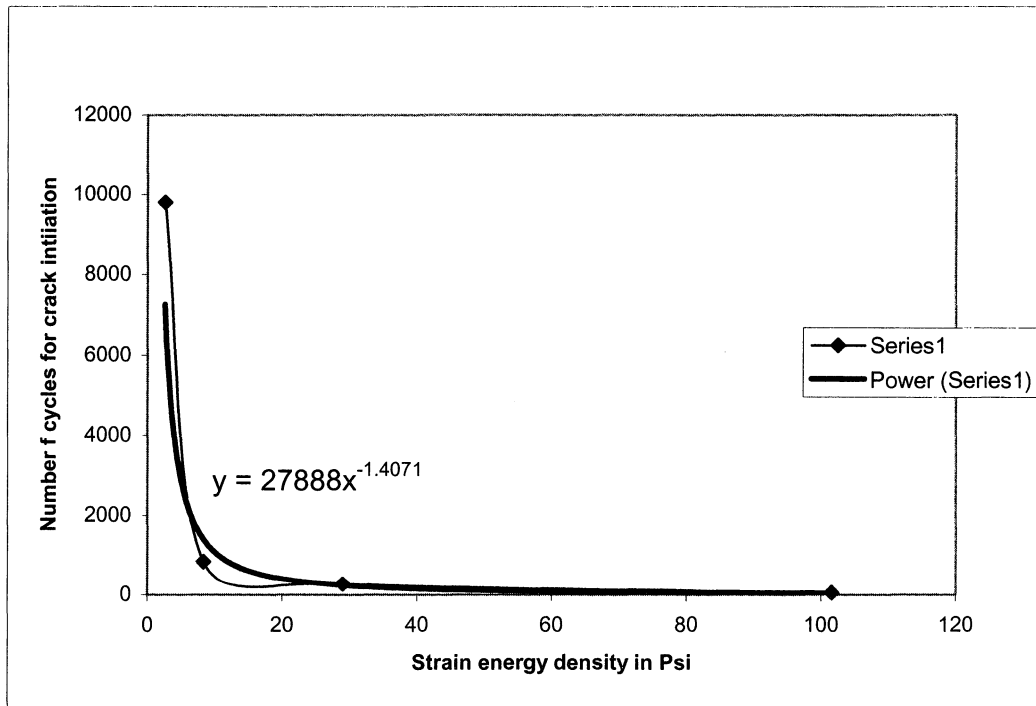


Figure 4-15 Number of Cycles to Crack Initiation vs Strain Energy Density per Cycle

From this exercise, strain energy density model for the estimation of fatigue life of 62Sn36Pb2Ag solder subjected to cyclic mechanical bending is defined by Equations 4-3, 4-4, and 4-5. This method is semi-empirical in nature because the constants are obtained from FEA and not from experiment.

$$\text{Number of cycles for crack initiation } N_0 = 27888 \Delta W^{-1.4071} \quad (4-3)$$

$$\text{Rate of crack propagation } da/dN = 4.96E-8 \Delta W^{1.13} \quad (4-4)$$

$$\text{Fatigue life } N_f = 138616 \Delta W^{-1.1295} \quad (4-5)$$

5 Conclusions and Recommendation for Future Research

In Section 4.0, a fatigue life model was developed by integrating computer simulation and strain energy density model. The implementation and advantages of this model is described in Section 5.2.

5.1 Discussion of Results

Equations 4-3, 4-4, and 4-5 together describe the fatigue life model of the solder balls under consideration. From equation 4-5 it is evident that as the strain energy density in a load cycle decreases, the assembly can sustain a large number of such load cycles, i. e. its fatigue life increases. This increase in fatigue life is significant when the strain energy density in a cycle drops below 10 psi (Figure 4-14). Geometric parameters like body size, pitch, package thickness; etc can be varied in such a way as to reduce the strain energy density during cyclic loading in order to design long lasting assemblies in electronic products.

5.2 Advantages of the Fatigue Model Developed in the Thesis

The experimental setup for three-point cyclic bending tests can be replaced with a finite element code capable of performing nonlinear elastic-plastic stress analysis and the ΔW value thus obtained can be substituted in the model developed in the thesis. This approach saves time, money, efforts, and reduce the need for destructive physical testing of the sample. Unlike the statistical models mentioned in Section 2. 1, this approach does not change with the type of package and technology. For instance, a Weibull distribution model based on the field data for failure rate in plastic BGA will be inapplicable to determine the failure rate in ceramic BGA. Such approaches need failure data for each

type of interconnection for a reasonable prediction of failure rate. The semi-empirical fatigue model developed in this thesis requires only the input of geometry, material properties, and operating conditions (for load and boundary conditions) along with a code capable of performing non-linear elastic-plastic stress analysis.

5.3 Recommendation for Future Work

A correlation between strain energy density and fatigue life has been obtained by computing ΔW at different values of applied displacement. This approach can be extended to determine the influence of various parameters on the fatigue life of BGA by conducting a parametric study to record the strain energy density (ΔW) with each individual variable parameter, and substituting the corresponding ΔW in the model developed in Section 4. 2. After the effect of each parameter is studied, empirical constants may be computed as a function of package geometry. Using this exercise, a subroutine may be developed that can suggest optimum geometry for an assembly to last for a specific number of cycles. For instance, if the application of an electronic device does not demand a large number of bending load cycles to be sustained, the resources that go into the product can be optimized using the subroutine. The current study is limited to considering other elements of the assembly like the PCB, die, substrate etc as elastic materials only. The inclusion of their plasticity properties may increase the fatigue life of the assembly. This case can be investigated in the future.

References

- Amkor Inc. (2001). *Effect of Simulation Methodology on Solder Joint Crack Growth Correlation*. Retrieved February 04, 2004, from http://www.amkor.com/products/notes_papers/RDARV_Article1200.pdf
- Bolotin, V. V. (1999). *Mechanics of Fatigue*. Boca Raton: CRC Press.
- Dieter, G. E. (1988). *Mechanical Metallurgy* (Metric ed.). London: McGraw-Hill Companies, Inc.
- Hsu, T.R. (1986). *The Finite Element Method in Thermomechanics*. London: Allen & Unwin, Inc.
- Iannuzzelli, R.J. & Seyyedi, J. (2001). Reliability of Micro-BGA Solder Joints – Predicted vs. Actual. *Proceedings of IPACK 2001, USA, 15500*, pp.1113-1120.
- Intel Inc. (2003). *Ball Grid Array (BGA) Packaging*. Retrieved September 21, 2003, from http://developer.intel.com/design/packtech/ch_14.pdf
- Kitano, M. (1997). Shape Prediction of Solder Bump Joint by Surface Tension Analysis and Fatigue strength Evaluation. *Advances in Electronic Packaging*, 2, 1407-1412.
- Lau, J. H. (Ed.). (1995). *Ball Grid Array Technology*. New York: McGraw-Hill Companies Inc.
- Lau, J. H. & Pao, Y. (1997). *Solder Joint Reliability of BGA, CSP, Flip Chip, and Fine Pitch SMT Assemblies*. New York: McGraw-Hill Companies, Inc.
- Lim, C. T., Seah, S. K. W., Tan, V. B. C. & Quah, S. E. (2003). Study of Microvia Failure Under PCB Flexing Loads [Electronic Version]. *Proceedings of the Electronic Components and Technology Conference, Hawaii*, pp. 95-99.

- National Institute of Standards and Technology. *Database for Solder Properties with Emphasis on New Lead-free Solders Release 4.0*. Retrieved March 29, 2004 from National Institute of Standards & Technology and Colorado School of Mines Online Access via: <http://www.boulder.nist.gov/div853/lead%20free/Part1.html#%201.1>
- National Institute of Standards and Technology. *Sn-Pb Properties and Models*. Retrieved March 29, 2004 from National Institute of Standards and Technology Online Access via: http://www.metallurgy.nist.gov/solder/clech/Sn-Pb_Creep.html
- Noghuchi, H., Kim, Y., and Amagai, M. (2003). Vibration Fatigue Reliability of BGA-IC package with Pb-free solder and Pb-Sn solder. *53rd Electronic Components & Technology, New Orleans*, pp. 891-897.
- Reed Electronics. (2000). *Surface Mount Technology*. Retrieved February 2003, from <http://www.reedelectronics.com/ednmag/contents/images/220402.pdf>
- Rao, R. T. (2001). *Fundamentals of Microsystems Packaging*. New York: McGraw-Hill Companies Inc.
- Syed, A. (2001). *Overview of Reliability Models and Data Needs*. Workshop on Modeling and Data Needs for Lead-Free Solders.
- Zhu, L. (2001). Sub modeling Technique for BGA Reliability Analysis of CSP Packaging Subjected to an Impact Loading. *Proceedings of IPACK'01, Hawaii, 15873*, pp.1401-1409.